Scientific Research Publishing

Applied Mathematics, 2023, 14, 612-651
https://www.scirp.org/journal/am
ISSN Online: 2152-7393
ISSN Print: 2152-7385

NCCT for Micropolar Solid and Fluid Media Based on Internal Rotations and Rotation Rates with Rotational Inertial Physics: Model Problem Studies

Karan S. Surana, Jacob K. Kendall

School of Mechanical Engineering, University of Kansas, Lawrence, Kansas, USA
Email: kssurana@ku.edu

How to cite this paper: Surana, K.S. and Kendall, J.K. (2023) NCCT for Micropolar Solid and Fluid Media Based on Internal Rotations and Rotation Rates with Rotational Inertial Physics: Model Problem Studies. *Applied Mathematics*, **14**, 612-651.
https://doi.org/10.4236/am.2023.149037

Received: August 8, 2023
Accepted: September 24, 2023
Published: September 27, 2023

Abstract

This paper presents model problem studies for micropolar thermoviscoelastic solids without memory and micropolar thermoviscous fluid using micropolar non-classical continuum theories (NCCT) based on internal rotations and rotation rates in which rotational inertial physics is considered in the derivation of the conservation and balance laws (CBL). The dissipation mechanism is due to strain rates as well as rotation rates. Model problems are designed to demonstrate and illustrate various significant aspects of the micropolar NCCT with rotational inertial physics considered in this paper. In case of micropolar solids, the translational and rotational waves are shown to coexist. In the absence of microconstituents (classical continuum theory, CCT) the internal rotations are a free field, hence have no influence on CCT. Absence of gradients of displacements and strains in micropolar thermoviscous fluid medium prohibits existence of translational waves as well as rotational waves even though the appearance of the mathematical model is analogous to the solids, but in terms of strain rates. It is shown that in case of micropolar thermoviscous fluids the BAM behaves more like time dependent diffusion equation *i.e.*, like heat conduction equation in Lagrangian description. The influence of rotational inertial physics is demonstrated using BLM as well as BAM in the model problem studies.

Keywords

Micropolar, Internal Rotations, Internal Rotation Rates, Translational Waves, Rotational Waves, Dissipation, Thermoviscous, Rotational Inertial Physics

1. Introduction, Literature Review and Scope of Current Work

In recent papers, Surana *et al.* [1] [2] have shown that micropolar NCCT for solid and fluid media based on internal rotations (due to deformation gradient tensor) and internal rotation rates (due to velocity gradient tensor) are thermodynamically and mathematically consistent. All other micropolar non-classical continuum theories based on Cosserat rotations and Cosserat rotation rates, those considering internal and Cosserat rotations and rotation rates, couple stress NCCT utilizing polynomial or potential functions approach for deriving constitutive theories are either in violation of thermodynamic consistency and/or mathematical consistency. In reference [3] Surana *et al.* extended the micropolar NCCT of reference [1] based on internal rotations for solid medium to account for rotational inertial physics. This leads to modification of balance of angular momenta (BAM) and balance of moment of moments (BMM) balance laws of reference [1]. Additionally, satisfying entropy inequality requires incorporating a constraint equation in the mathematical model consisting of CBL and the constitutive theories. Authors showed (without model problem studies) that this mathematical model permits co-existence of translational and rotational waves. In reference [4] Surana *et al.* extended the micropolar NCCT of reference [2] for fluids to include rotational inertial physics. This also resulted in modification of the CBL presented in reference [2]. Authors in references [3] [4] showed that the requirement of satisfying entropy inequality necessitated that a constraint equation be considered as part of the mathematical model based on CBL and the constitutive theories. Authors discussed (without model problem studies) similarity of BAM in rotation rates in the case of micropolar fluids [4] with the BAM for micropolar solids in rotations in reference [3], but lack of rotational waves in micropolar fluids due to absence of stiffness (due to lack of strain physics). Influence of rotational inertial physics on the evolution of the IVPs in general resulting due to micropolar NCCT was not discussed. Unfortunately, there are not many published works on micropolar NCCT that consider rotational inertial physics. References [5] [6] consider flow of micropolar fluids through porous medium and dynamics of hydro-magnetic flow of micropolar fluids.

The objective of this paper is to present model problem studies for micropolar solids and micropolar fluids using the mathematical model consisting of the CBL and the constitutive theories for micropolar non-classical solids and fluids with rotational inertial physics presented in references [3] [4]. Model problem studies are intentionally kept simple (one dimensional as far as possible) so that the contributions of rotational inertial physics can be clearly illustrated and established.

2. Mathematical Models

In the following, we consider complete 3D mathematical models consisting of

CBL and the constitutive theories for micropolar non-classical solid and fluids based on internal rotations and internal rotation rates with rotational inertial physics presented by Surana *et al.* [3] [4]. In both cases, we consider thermo-viscous physics in which the dissipation mechanism is due to rate of strain (solids) and strain rate (fluids) as well as due to rate of symmetric part of rotation gradient tensor (solids) as well as due to symmetric part of rotational gradient rates (fluids).

2.1. Micropolar Thermoviscous Elastic Solid (Without Memory)

For small strain, small deformation physics the CBL and the constitutive theories presented in reference [3] modified for dissipation due to rate of strain (CCM) and rate of symmetric part of rotation gradient tensor (micropolar NCCT) are given by

$$\rho_0 \frac{D^2 u_k}{Dt^2} - \rho_0 F_k^b - \frac{\partial \sigma_{jk}}{\partial x_j} = 0 \tag{1}$$

$${}^{\Theta}I_0 \rho_0 \frac{D^2 \left({}_i\Theta_k\right)}{Dt^2} - \epsilon_{ijk}\sigma_{ij} - \frac{\partial m_{jk}}{\partial x_j} = 0 \tag{2}$$

$$\epsilon_{jkl}\left({}^{\Theta}I_0 \rho_0 v_j \left({}_i\omega_k\right) - m_{jk}\right) = 0 \tag{3}$$

$$\rho_0 \frac{De}{Dt} + \frac{\partial q_i}{\partial x_i} - \operatorname{tr}\left(\left[{}_s\sigma\right]\left[\dot{\varepsilon}\right]\right) - \operatorname{tr}\left(\left[{}_s m\right]\left[{}^{i\Theta}_{s}\dot{J}\right]\right) - \operatorname{tr}\left(\left[{}_a m\right]\left[{}^{i\Theta}_{a}\dot{J}\right]\right) = 0 \tag{4}$$

$$\text{Additive decomposition of } \boldsymbol{\sigma}\text{: } \boldsymbol{\sigma} = {}_s\boldsymbol{\sigma} + {}_a\boldsymbol{\sigma};\ \ {}_s\boldsymbol{\sigma} = {}^{d}_{s}\boldsymbol{\sigma} + {}^{e}_{s}\boldsymbol{\sigma} \tag{5}$$

$${}^{d}_{s}\boldsymbol{\sigma} = \sigma_0\big|_{\underline{\Omega}}\, \boldsymbol{I} + 2\mu\boldsymbol{\varepsilon} + \lambda\left(\operatorname{tr}\left(\boldsymbol{\varepsilon}\right)\right)\boldsymbol{I} + 2\eta\dot{\boldsymbol{\varepsilon}} + \kappa\operatorname{tr}\left(\dot{\boldsymbol{\varepsilon}}\right)\boldsymbol{I} \tag{6}$$

$${}_s\boldsymbol{m} = 2\mu_m\left({}^{i\Theta}_{s}\boldsymbol{J}\right) + 2\eta_m\left({}^{i\Theta}_{s}\dot{\boldsymbol{J}}\right) \tag{7}$$

$$\boldsymbol{q} = -\kappa\boldsymbol{g} \tag{8}$$

In the mathematical model we have a total of 25 equations BLM(3), BAM(3), BMM(3), FLT(1), constitutive theories for ${}_s\boldsymbol{\sigma}(6)$, ${}_s\boldsymbol{m}(6)$, $\boldsymbol{q}(3)$ in a total of 25 dependent variables $\boldsymbol{u}(3)$, ${}^{d}_{s}\boldsymbol{\sigma}(6)$, ${}_a\boldsymbol{\sigma}(3)$, ${}_s\boldsymbol{m}(6)$, ${}_a\boldsymbol{m}(3)$, $\boldsymbol{q}(3)$, $\theta(1)$ hence the model has closure. The last term in the entropy inequality

$$\frac{\boldsymbol{q}:\boldsymbol{g}}{\theta} - {}^{d}_{s}\boldsymbol{\sigma}:\dot{\boldsymbol{\varepsilon}} - {}_s\boldsymbol{m}:{}^{i\Theta}_{s}\dot{\boldsymbol{J}} - {}_a\boldsymbol{m}:{}^{i\Theta}_{a}\dot{\boldsymbol{J}} \le 0 \tag{9}$$

must be set to zero to ensure that (9) is always satisfied. Then, in addition to (1)-(8). We must also satisfy

$${}_a\boldsymbol{m}:{}^{i\Theta}_{a}\dot{\boldsymbol{J}} = 0 \tag{10}$$

Equation (10) serves as a constraint on the mathematical Model (1)-(8).

2.2. Micropolar Thermoviscous Fluid Medium

We consider incompressible micropolar thermoviscous fluid medium. The CBL and constitutive theories of reference [4] are considered. These naturally include dissipation mechanism due to classical as well as non-classical micropolar phys-

ics. Following reference [4] we have the following for CBL and constitutive theories.

$$\frac{D\overline{\rho}}{Dt}+\overline{\rho}\,\mathrm{div}\left(\overline{\boldsymbol{v}}\right)=0\left(\mathrm{CM}\right)\quad(\mathrm{CM}) \tag{11}$$

$$\overline{\rho}\frac{\partial\overline{\boldsymbol{v}}}{\partial t}+\overline{\rho}\left(\overline{\boldsymbol{v}}:\overline{\boldsymbol{\nabla}}\right)\overline{\boldsymbol{v}}-\overline{\rho}\overline{\boldsymbol{F}}^{b}-\overline{\boldsymbol{\nabla}}:\overline{\boldsymbol{\sigma}}^{(0)}=0\quad(\mathrm{BLM}) \tag{12}$$

$${}^{\Theta}\overline{I}\,\overline{\rho}\frac{D}{Dt}\left({}_{i}\overline{\omega}_{k}\right)-\epsilon_{ijk}\overline{\sigma}_{ij}^{(0)}-\overline{m}_{mk,m}^{(0)}=0\quad(\mathrm{BAM}) \tag{13}$$

$$\epsilon_{jkl}\left({}^{\Theta}\overline{I}\,\overline{\rho v}_{j}\left({}_{i}\overline{\omega}_{k}\right)-\overline{m}_{jk}^{(0)}\right)=0\quad(\mathrm{BMM}) \tag{14}$$

$$\overline{\rho}\frac{D\overline{e}}{Dt}+\overline{\boldsymbol{\nabla}}:\overline{\boldsymbol{q}}-{}_{s}\overline{\boldsymbol{\sigma}}^{(0)}:\overline{\boldsymbol{D}}-{}_{s}\overline{\boldsymbol{m}}^{(0)}:{}_{s}^{f}\overline{\boldsymbol{J}}-{}_{a}\overline{\boldsymbol{m}}^{(0)}:{}_{a}^{f}\overline{\boldsymbol{J}}=0\quad(\mathrm{FLT}) \tag{15}$$

$$\overline{\rho}\left(\frac{D\overline{\Phi}}{Dt}+\overline{\eta}\frac{D\overline{\theta}}{Dt}\right)+\frac{\overline{\boldsymbol{q}}:\overline{\boldsymbol{g}}}{\overline{\theta}}-{}_{s}\overline{\boldsymbol{\sigma}}^{(0)}:\overline{\boldsymbol{D}}-{}_{s}\overline{\boldsymbol{m}}^{(0)}:{}_{s}^{f}\overline{\boldsymbol{J}}-{}_{a}\overline{\boldsymbol{m}}^{(0)}:{}_{a}^{f}\overline{\boldsymbol{J}}\le 0\quad(\mathrm{SLT}) \tag{16}$$

$${}_{s}^{d}\overline{\boldsymbol{\sigma}}^{(0)}=\overline{\boldsymbol{s}}\big|_{\underline{\Omega}}+2\eta\overline{\boldsymbol{D}}+\kappa\left(\mathrm{tr}\left(\overline{\boldsymbol{D}}\right)\right)\boldsymbol{I} \tag{17}$$

$$\text{Additive decomposition of }\overline{\boldsymbol{\sigma}}^{(0)}:\ \overline{\boldsymbol{\sigma}}^{(0)}={}_{s}\overline{\boldsymbol{\sigma}}^{(0)}+{}_{a}\overline{\boldsymbol{\sigma}}^{(0)};\ {}_{s}\overline{\boldsymbol{\sigma}}^{(0)}={}_{s}^{d}\overline{\boldsymbol{\sigma}}^{(0)}+{}_{s}^{e}\overline{\boldsymbol{\sigma}}^{(0)} \tag{18}$$

$${}_{s}\overline{\boldsymbol{m}}^{(0)}=2\eta_{m}\left({}_{s}^{f}\overline{\boldsymbol{J}}\right) \tag{19}$$

$$\overline{\boldsymbol{q}}=-\kappa\overline{\boldsymbol{g}} \tag{20}$$

where

$${}_{i}\overline{\boldsymbol{\omega}}={}_{i}^{r}\overline{\boldsymbol{\Theta}},\quad\frac{D\left({}_{i}\overline{\boldsymbol{\omega}}\right)}{Dt}={}_{i}^{r}\dot{\overline{\boldsymbol{\Theta}}} \tag{21}$$

In this mathematical model we have CM(1), BLM(3), BAM(3), BMM(3), FLT(1) and the constitutive theories for ${}_{s}^{d}\overline{\boldsymbol{\sigma}}^{(0)}(6)$, ${}_{s}\overline{\boldsymbol{m}}^{(0)}(6)$, $\overline{\boldsymbol{q}}(3)$, a total of 26 equations in 26 dependent variables $\overline{\rho}(1)$, $\overline{\boldsymbol{v}}(3)$, ${}_{s}^{d}\overline{\boldsymbol{\sigma}}^{(0)}(6)$, ${}_{a}\overline{\boldsymbol{\sigma}}^{(0)}(3)$, ${}_{s}\overline{\boldsymbol{m}}^{(0)}(6)$, ${}_{a}\overline{\boldsymbol{m}}^{(0)}(3)$, $\overline{\boldsymbol{q}}(3)$, $\overline{\theta}(1)$. The last term in the entropy inequality must be set to zero to ensure that (16) is not violated. Thus

$${}_{s}\overline{\boldsymbol{m}}^{(0)}:{}_{a}^{f}\overline{\boldsymbol{J}}=0 \tag{22}$$

must serve as constraint, hence constitutes additional condition that must be satisfied to guarantee that the entropy inequality is not violated.

3. Model Problems

In this section, we consider model problems for micropolar solid and fluid media. Model problems are intentionally kept simple so that significant features of micropolar aspects in the presence of rotational inertial physics can be demonstrated.

3.1. Translational and Rotational Waves in Micropolar Solids

The objective of this study is to demonstrate existence of pure rotational waves in micropolar solids with rotational inertial physics. Just like in classical continuum mechanics (CCM) we can show existence, propagation, reflection and in-

teraction of translational (stress) waves, in case of micropolar solids with rotational inertial physics we can additionally show existence, propagation, reflection and interaction of rotational (moment) waves. That is, in micropolar solids with rotational inertial physics, translational and rotational waves coexist. In the following study we consider purely one dimensional case of BLM and BAM. In the studies presented here we show that BLM permits translational waves where as BAM with rotational inertial physics permits pure rotational waves.

Mathematical models

One dimensional form of BLM and balance of angular momenta with rotational inertial physics (Equations (1) and (2)) for small strain small deformation and the associated constitutive theories for thermoviscoelastic (without memory) micropolar solid with dissipation mechanism due to rate of strain (CCM) and due to rate of symmetric part of the rotation gradient tensor are given by (in the absence of body forces, body moments, initial stress and equilibrium Cauchy stress, thus $\sigma_{11} = {}_s\sigma_{11} = {}^d_s\sigma_{11}$ and using x for x_1)

$$\rho_0 \frac{\partial^2 u_1}{\partial t^2} - \frac{\partial \left({}^d_s\sigma_{11} \right)}{\partial x} = 0 \tag{23}$$

$${}^{\Theta}I_0\rho_0 \frac{\partial^2 \left({}_i\Theta_1 \right)}{\partial t^2} - \frac{\partial {}_s m_{11}}{\partial x} = 0 \tag{24}$$

$${}^d_s\sigma_{11} = \left(2\mu + \lambda \right) \frac{\partial u_1}{\partial x} + \left(2\eta + \kappa \right) \frac{\partial}{\partial t} \left(\frac{\partial u_1}{\partial x} \right) \tag{25}$$

$${}_s m_{11} = \left(\alpha_1 \right) \frac{\partial \left({}_i\Theta_1 \right)}{\partial x} + \left(\alpha_2 \right) \frac{\partial}{\partial t} \left(\frac{\partial \left({}_i\Theta_1 \right)}{\partial x} \right) \quad \alpha_1 = \mu_m, \alpha_2 = \eta_m \tag{26}$$

Substituting (25) in (23) and (26) in (24) we obtain

$$\rho_0 \frac{\partial^2 u_1}{\partial t^2} - \left(2\mu + \lambda \right) \frac{\partial^2 u_1}{\partial x^2} - \left(2\eta + \kappa \right) \frac{\partial}{\partial t} \left(\frac{\partial^2 u_1}{\partial x^2} \right) = 0 \tag{27}$$

$${}^{\Theta}I_0\rho_0 \frac{\partial^2 \left({}_i\Theta_1 \right)}{\partial t^2} - \left(\alpha_1 \right) \frac{\partial^2 \left({}_i\Theta_1 \right)}{\partial x^2} - \left(\alpha_2 \right) \frac{\partial}{\partial t} \left(\frac{\partial^2 \left({}_i\Theta_1 \right)}{\partial x^2} \right) = 0 \tag{28}$$

for 1D case and for incompressible physics $2\mu + \lambda = E$, modulus of elasticity, as Poison's ratio $\nu = 0$ and $\kappa = 0$, hence (28) reduces to (but (28) remains same).

$$\rho_0 \frac{\partial^2 u_1}{\partial t^2} - E \frac{\partial^2 u_1}{\partial x^2} - 2\eta \frac{\partial}{\partial t} \left(\frac{\partial^2 u_1}{\partial x^2} \right) = 0 \tag{29}$$

$${}^{\Theta}I_0\rho_0 \frac{\partial^2 \left({}_i\Theta_1 \right)}{\partial t^2} - \left(\alpha_1 \right) \frac{\partial^2 \left({}_i\Theta_1 \right)}{\partial x^2} - \left(\alpha_2 \right) \frac{\partial}{\partial t} \left(\frac{\partial^2 \left({}_i\Theta_1 \right)}{\partial x^2} \right) = 0 \tag{30}$$

Remarks

1) Equation (29) describes translational or ${}^d_s\sigma_{11}$ stress wave in a viscous elastic medium. In the absence of the last term in (29), (29) represents translational waves in inviscid elastic medium. Dissipation (last term in (29)) results in amplitude decay and base elongation.

2) Equation (30) is analogous to equation (29) and can be obtained b replac-

ing u_1, ρ_0, E, and 2η in (29) by ${}_i\Theta_1$, ${}^{\Theta}I_0\rho_0$, α_1 and α_2. Thus, (30) describes rotational waves *i.e.*, moment (${}_sm_{11}$) wave. The third term in (30) is due to micropolar dissipation physics which would result in amplitude decay and base elongation of ${}_sm_{11}$ rotational wave.

3) We note the lack of coupling between (29) and (30) due to zero antisymmetric part of the deviatoric Cauchy stress. This is not the case in 2D and 3D applications.

4) Presence of (29) and (30) confirm coexistence of translational and rotational waves in micropolar elastic solids.

Dimensionless form of the mathematical model

We first nondimensionalize (29) and (30) before presenting their solutions. We write (29) and (30) with hat ($\wedge$) on all quantities indicating that all quantities have their usual dimensions (units)

$$\hat{\rho}_0\frac{\partial^2\hat{u}_1}{\partial\hat{t}^2}-\hat{E}\frac{\partial^2\hat{u}_1}{\partial\hat{x}^2}-2\hat{\eta}\frac{\partial}{\partial\hat{t}}\left(\frac{\partial^2\hat{u}_1}{\partial\hat{x}^2}\right)=0 \tag{31}$$

$${}^{\Theta}I_0\hat{\rho}_0\frac{\partial^2\left({}_i\hat{\Theta}_1\right)}{\partial\hat{t}^2}-\left(\hat{\alpha}_1\right)\frac{\partial^2\left({}_i\hat{\Theta}_1\right)}{\partial\hat{x}^2}-\left(\hat{\alpha}_2\right)\frac{\partial}{\partial\hat{t}}\left(\frac{\partial^2\left({}_i\hat{\Theta}_1\right)}{\partial\hat{x}^2}\right)=0 \tag{32}$$

We note that in general the speed of translational wave is different than the speed of rotational wave. However, since in this case (31) and (32) are decoupled, it is possible to nondimensionalize (31) and (32) such that in the dimensionless domain the speed of prorogation of both translation and rotational waves is unity. Obviously in 2D and 3D cases it is not possible to do so. We present details in the following.

BLM: Model TW1

Choosing L_0, η_0, $(\rho_0)_{ref}$, t_0, $v_0=L_0/t_0=\sqrt{\dfrac{E_0}{\rho_0}}$ and $E_0=(\rho_0)_{ref}v_0^2$ as reference quantities in which v_0 is the speed of translational wave (speed of sound in CCM).

$$\rho_0\frac{\partial^2u_1}{\partial t^2}-E\frac{E_0}{(\rho_0)_{ref}v_0^2}\frac{\partial^2u_1}{\partial x^2}-\frac{2\eta}{Re}\frac{\partial}{\partial t}\left(\frac{\partial^2u_1}{\partial x^2}\right)=0 \tag{33}$$

where $1/Re=\dfrac{\eta_0}{L_0(\rho_0)_{ref}v_0}$, Reynolds number. If we choose $(\rho_0)_{ref}=\hat{\rho}_0$, $E_0=\hat{E}=(\rho_0)_{ref}v_0^2$ and $C_d=\dfrac{2\eta}{Re}$ as damping coefficient, then (33) can be reduced to

$$\frac{\partial^2u_1}{\partial t^2}-\frac{\partial^2u_1}{\partial x^2}-c_d\frac{\partial}{\partial t}\left(\frac{\partial^2u_1}{\partial x^2}\right)=0 \tag{34}$$

In (34), the dimensionless speed of sound (based on reference quantities) in an inviscid medium is unity. We use (34) in the numerical studies.

BAM: Using speed of rotational waves as reference velocity: Model RW1

In this case, when nondimensionalizing BAM we choose speed of rotational

wave as reference velocity. We also choose some of the same reference quantities as in BLM except we choose $\left({}^{\Theta}I_0\right)_{ref}$, $\left(\alpha_1\right)_0$, $\left(\alpha_2\right)_0$, $\omega_0 = \sqrt{\left(\alpha_1\right)_0 \Big/ \left({}^{\Theta}I_0\right)_{ref}\left(\rho_0\right)_{ref}}$ and $t_0 = L_0/\omega_0$, $\left(\alpha_1\right)_0 = \left({}^{\Theta}I_0\right)_{ref}\left(\rho_0\right)_{ref}\omega_0^2$, then (32) can be written as

$$ {}^{\Theta}I_0\rho_0\frac{\partial^2\left({}_i\Theta_1\right)}{\partial t^2} - \left(\alpha_1\right)\frac{\left(\alpha_1\right)_0}{\left({}^{\Theta}I_0\right)_{ref}\left(\rho_0\right)_{ref}\omega_0^2}\frac{\partial^2\left({}_i\Theta_1\right)}{\partial x^2} - \left(\alpha_2\right)\frac{1}{Re^*}\frac{\partial}{\partial t}\left(\frac{\partial^2\left({}_i\Theta_1\right)}{\partial x^2}\right) = 0 \quad (35) $$

If $\left({}^{\Theta}I_0\right)_{ref} = {}^{\Theta}\hat{I}_0$, $\left(\rho_0\right)_{ref} = \hat{\rho}_0$, then (35) can be reduced to

$$ \frac{\partial^2\left({}_i\Theta_1\right)}{\partial t^2} - \frac{\partial^2\left({}_i\Theta_1\right)}{\partial x^2} - \frac{\left(\alpha_2\right)}{Re^*}\frac{\partial}{\partial t}\left(\frac{\partial^2\left({}_i\Theta_1\right)}{\partial x^2}\right) = 0 \quad (36) $$

in which $Re^* = \dfrac{\left({}^{\Theta}I_0\right)_{ref}\left(\rho_0\right)_{ref}\omega_0 L_0}{\left(\alpha_2\right)_0}$ is the Reynolds number associated with dissipation due to micropolar physics. If we define $c_d^* = \dfrac{\alpha_2}{Re^*}$ as the dissipation coefficient due to micropolar physics, then (36) can be written as

$$ \frac{\partial^2\left({}_i\Theta_1\right)}{\partial t^2} - \frac{\partial^2\left({}_i\Theta_1\right)}{\partial x^2} - c_d^*\frac{\partial}{\partial t}\left(\frac{\partial^2\left({}_i\Theta_1\right)}{\partial x^2}\right) = 0 \quad (37) $$

Equation (34) and (37) are the simplified dimensionless forms of BLM and BAM describing translational and rotational waves in the presence of dissipation mechanisms. In the numerical studies we use equations (34) and (37).

BAM: Using translation wave speed as reference velocity: Model RW2

In this case we choose

$$ \left.\begin{aligned} v_0 &= \sqrt{\frac{E_0}{\left(\rho_0\right)_{ref}}} \\ t_0 &= \frac{L_0}{v_0} \end{aligned}\right\} \quad (38) $$

using these reference values we can nondimensionalize (32) as follows.

$$ \begin{aligned} &{}^{\Theta}I_0\rho_0\frac{\partial^2\left({}_i\Theta_1\right)}{\partial t^2} - \left(\alpha_1\right)\frac{\left(\alpha_1\right)_0}{\left({}^{\Theta}I_0\right)_{ref}\left(\rho_0\right)_{ref}v_0^2}\frac{\partial^2\left({}_i\Theta_1\right)}{\partial x^2} \\ &-\left(\alpha_2\right)\frac{\left(\alpha_2\right)_0}{\left({}^{\Theta}I_0\right)_{ref}\left(\rho_0\right)_{ref}L_0v_0}\frac{\partial}{\partial t}\left(\frac{\partial^2\left({}_i\Theta_1\right)}{\partial x^2}\right) = 0 \end{aligned} \quad (39) $$

If we choose $\left({}^{\Theta}I_0\right)_{ref} = {}^{\Theta}\hat{I}_0$, $\left(\rho_0\right)_{ref} = \hat{\rho}_0$ and define

$$ \alpha_1^* = \frac{\left(\alpha_1\right)_{0/2}}{\left({}^{\Theta}I_0\right)_{ref}\left(\rho_0\right)_{ref}v_0^2}, \quad c_d^* = \frac{\alpha_2}{Re^*}, \quad 1/Re^* = \frac{\left(\alpha_2\right)_0}{\left({}^{\Theta}I_0\right)_{ref}\left(\rho_0\right)_{ref}L_0v_0} $$

then (39) can be reduced to

$$ \frac{\partial^2\left({}_i\Theta_1\right)}{\partial t^2} - \alpha_1^*\frac{\partial^2\left({}_i\Theta_1\right)}{\partial x^2} - c_d^*\frac{\partial}{\partial t}\left(\frac{\partial^2\left({}_i\Theta_1\right)}{\partial x^2}\right) = 0 \quad (40) $$

In this case the speed of dimensionless rotational wave is $\sqrt{\alpha_1^*}$ which may not be unity. We use (40) in the numerical studies.

Remarks

1) We consider (34), (37) and (40) for presenting numerical studies.

2) Numerical studies are presented using space-time coupled finite element method based on space-time residual functional for a space-time strip with time marching [5] in which space-time local approximation for a space-time element are p-version hierarchical with higher order global differentiability in space and time.

3) We recast (34), (37) and (40) as a system of first order PDEs for convenience of defining BCs and ICs.

First order system of PDEs

Translational (or stress) waves (Model TW1)

We recast (34) as follows

$$\left.\begin{aligned} &\frac{\partial v_1}{\partial t}-\frac{\partial\left({}^{d}_{s}\sigma_{11}\right)}{\partial x}=0\\ &{}^{d}_{s}\sigma_{11}-\frac{\partial u_1}{\partial x}-c_d\frac{\partial v_1}{\partial x}=0\\ &v_1-\frac{\partial u_1}{\partial t}=0 \end{aligned}\right\} \tag{41}$$

Rotational (or moment) waves (Model RW1)

We recast (37) as

$$\left.\begin{aligned} &\frac{\partial\left({}_{i}\omega_1\right)}{\partial t}-\frac{\partial\left({}_{s}m_{11}\right)}{\partial x}=0\\ &{}_{s}m_{11}-\frac{\partial\left({}_{i}\Theta_1\right)}{\partial x}-c_d^*\frac{\partial\left({}_{i}\omega_1\right)}{\partial x}=0\\ &{}_{i}\omega_1-\frac{\partial\left({}_{i}\Theta_1\right)}{\partial t}=0 \end{aligned}\right\} \tag{42}$$

Rotational (or moment) waves (Model RW2)

$$\left.\begin{aligned} &\frac{\partial\left({}_{i}\omega_1\right)}{\partial t}-\frac{\partial\left({}_{s}m_{11}\right)}{\partial x}\\ &{}_{s}m_{11}-\alpha_1^*\frac{\partial\left({}_{i}\Theta_1\right)}{\partial x}-c_d^*\frac{\partial\left({}_{i}\omega_1\right)}{\partial x}=0\\ &{}_{i}\omega_1-\frac{\partial\left({}_{i}\Theta_1\right)}{\partial t}=0 \end{aligned}\right\} \tag{43}$$

Numerical studies

Evolutions are computed for models TW1, RW1 and RW2 using space-time coupled finite element method for a space-time strip with time marching [7]. The space-time local approximation for a space-time element is p-version hierarchical with higher order global differentiability in space and time. Discretizations, p-levels and the minimally confirming spaces are chosen such that for each space-time strip the space-time residual functional for the discretization is

$O(10^{-8})$ or lower ensuring that PDEs are satisfied accurately by the computed solution. In the present studies we choose a uniform mesh of 30, nine node p-version hierarchical finite elements with p-levels of 9 in space and time for all elements of the space-time strip. We choose local approximations in space and time of class C^{11}.

A time increment of $\Delta t = 0.1$ is used in all computations. The solution is computed for the first space-time strip ($0 \le t \le \Delta t$) and then time marched to obtain evolution for desired value of τ (final value of time). Since all evolutions considered here are smooth, choice of solutions of class C^{11} in space and time suffices. For this choice of the order of the approximation space, the space-time integrals for the discretization of the space-time strip are Riemann. The 30 element uniform discretization with p-levels of 9 for space and time and $k = 2$ for both space and time, yield space-time residual functional values for each space-time strip of the order $O(10^{-8})$ or lower during the entire evolution, confirming good accuracy of the computed solution. In the following, we present computed evolutions for: translation wave using Model TW1 and rotations wave using Models TR1 and TR2.

Figure 1 shows schematic, space-time domain $\bar{\Omega}_{xt}$, discretization $\bar{\Omega}_{xt}^{T} = \bigcup_e \bar{\Omega}_{xt}^{(e)}$ of the space time domain into space-time strips, discretization $\left(\bar{\Omega}_{xt}^{(1)}\right)^{T} = \bigcup_e \bar{\Omega}_{xt}^{(e)}$ of the first space-time strip $\bar{\Omega}_{xt}^{(1)}$ and the details of stress ${}^{d}_{s}\sigma_{11}$ boundary conditions (for TW1) applied to the last space-time element face at $x = 1$. In the numerical studies, we choose negative σ_0 (compressive) for the applied pulse at $x = 1$. The details of applying BC at $x = L$ for mathematical models RW1 and RW2 are similar.

Translational wave: Model TW1

We consider mathematical model TW1. Evolution is computed for 30 time steps for the undamped case, $c_d = 0$ using space-time coupled finite element formulation based on space-time residual functional. Since in this case, the speed of wave propagation is one, in ten time steps with $\Delta t = 0.1$, the applied pulse at $x = 1$ reaches the impermeable boundary at $x = 0$. Due to zero damping, we expect the applied pulse shape to be preserved during evolution. **Figure 2(a)** shows a plot of ${}^{d}_{s}\sigma_{11}$ versus x for various values of time. Time steps 2, 6, 10 show the incident compressive pulse entering the spatial domain at $x = L$ and propagating without amplitude decay or base elongation confirming the absence of numerical dispersion. At the 10th time step the compressive pulse is precisely at $x = 0$ as expected. Reflection of the compressive incident pulse at the impermeable boundary (at $x = 0$) results in reflected compressive pulse at the 11th time step with double the peak value. Upon further evolution the reflected compressive pulse recovers its peak and base at the 12th time step (not shown). At the 14th time step, we see reflected pulse with the same amplitude and base as the original incident pulse propagating toward the right end. At the 20th time step the reflected compressive pulse reaches the free boundary at $x = L = 1$ and

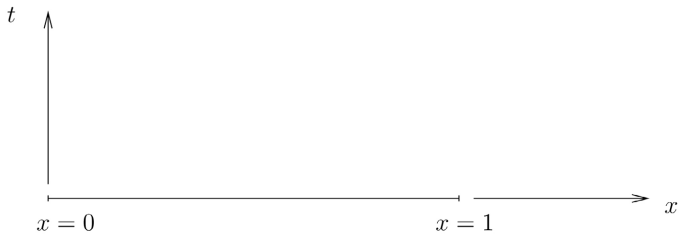

(a) schematic of spatial domain

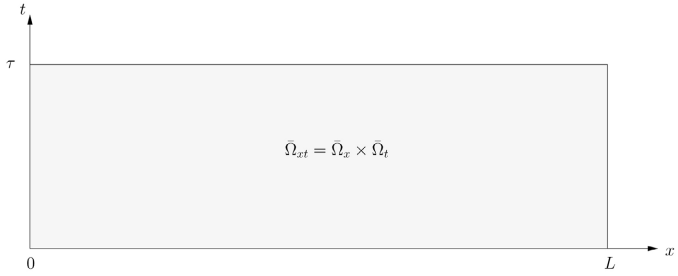

(b) Space time domain $\bar{\Omega}_{xt}$

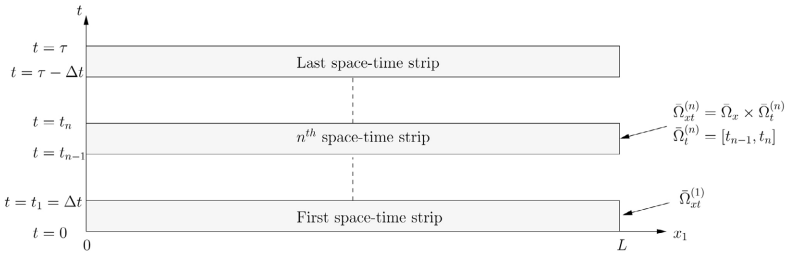

(c) Discretization $\bar{\Omega}_{xt}^{T} = \bigcup_i \bar{\Omega}_{xt}^{(i)}$ in space-time strips

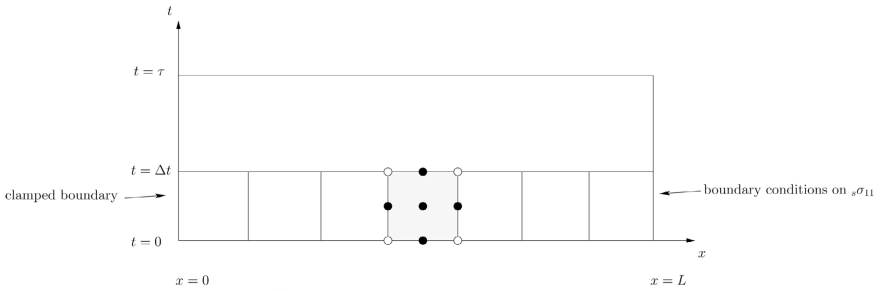

(d) Discretization $\left(\bar{\Omega}_{xt}^{(1)}\right)^{T} = \bigcup_e \bar{\Omega}_{xt}^{(e)}$ of the first space-time strip $\bar{\Omega}_{xt}^{(1)}$

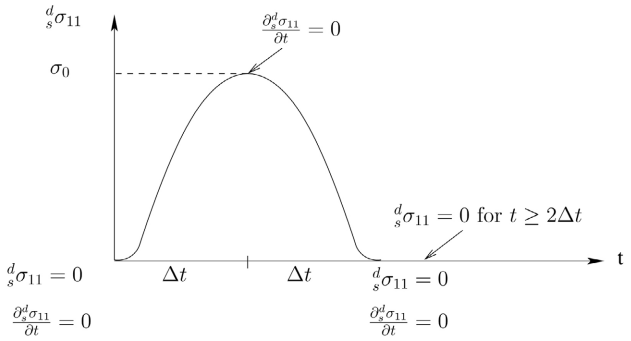

(e) ${}_s^d\sigma_{11}(t)$ as a function of time for $0 \leq t \leq 2\Delta t$ and for $t \geq 2\Delta t$

Figure 1. Spatial domain, space-time domain, Discretization into space-time strips, First space-time strip, Boundary conditions.

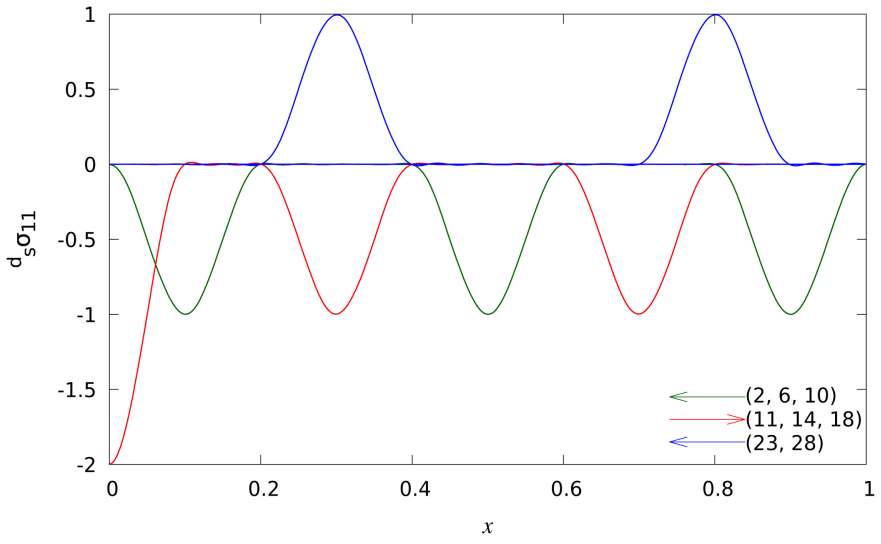

(a) Undamped case ($c_d = 0$)

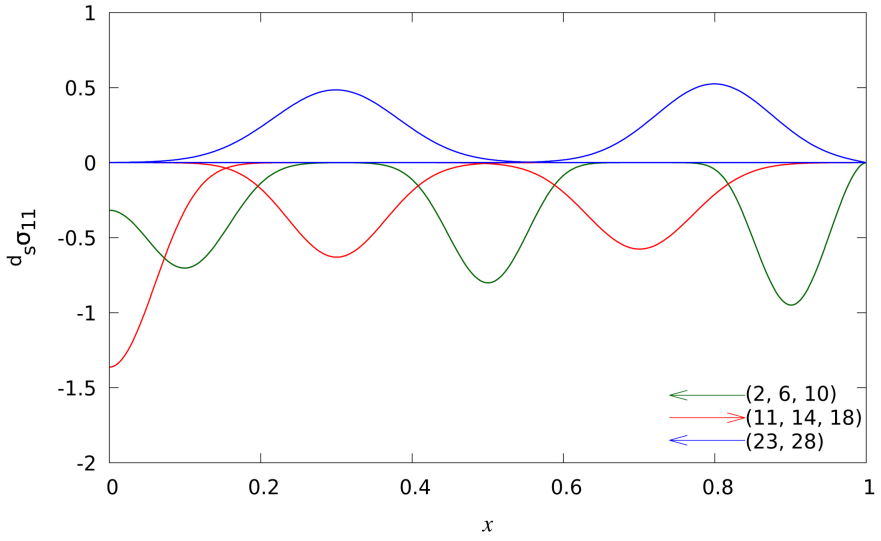

(b) Damped case ($c_d = 0.002$)

Figure 2. Evolution of deviatoric stress wave: $_s^d\sigma_{11}$ versus position x (Model TW1).

reflects as a tensile pulse of the same amplitude and base as the original incident pulse propagating towards the boundary at $x = 0$ (time steps 23 and 28 in **Figure 2(a)**).

In the next study for TW1, we consider dimensionless damping coefficient $c_d = 0.002$. **Figure 2(b)** shows evolution of $_s^d\sigma_{11}$ versus x for time steps 2, 6, 10; 11, 14, 18; 23 and 28 (same as in **Figure 2(a)** for the undamped case). In the incident pulse, amplitude decays and the base elongates during propagation (time steps 2, 6, 10). During reflection (time step 11), the magnitude of the pulse increases but recovers upon further evolution (time step 14). The reflected pulse reaches the free boundary and reflection from the free boundary results in a tensile pulse that propagates to the left. We observe the amplitude decay is more pronounced in the propagating incident pulse. The reflected pulses also shows

some amplitude decay, but the base elongation in the reflected pulse is more pronounced. All evolutions are smooth i.e., free of oscillations. Integrated sum of squares of the space-time residual functional are of the order of $O(10^{-8})$ or lower for each space-time strip ensuring that the computed solution is accurate. Choice of $k=2$ (order of the approximation space in space and time) is minimally conforming for the first order system of PDEs, hence all space-time integrals for $\left(\bar{\Omega}_{xt}^{(i)}\right)^T$, discretization of space-time strip $\bar{\Omega}_{xt}^{(i)}$ are Riemann. The space-time residual functional of the order $O(10^{-8})$ ensures that the PDEs are satisfied in point wise sense over each space-time strip discretization $\bar{\Omega}_{xt}^{(i)}$, hence good time accuracy of the evolution is ensured.

Rotational wave: Model RW1

We consider mathematical model RW1 defined by Equation (42). In this case, the equations are nondimensionalized using the speed of rotational wave, hence the dimensionless speed of the rotational wave is one. In the first study, we apply moment pulse *i.e.*, ${}_s m_{11}$ pulse of time duration $2\Delta t$ (similar to ${}_s^d\sigma_{11}$ shown in **Figure 1(e)**). We choose p-levels of 9 in space and time, $\Delta t=0.1$ and order *k* of the approximation space in space and time is chosen to be 2, which is minimally confirming for a first order system of PDEs. We choose peak values of ${}_s m_{11}=-1$. Evolution is computed using space-time strip with time marching, Integral form in space-time finite element process is based on space-time residual functional. **Figure 3(a)** shows the evolution for $c_d^*=0$ (undamped case). Incident moment pulse propagates towards the impermeable boundary without amplitude decay and base elongation. Upon reflection at $x=0$, the peak amplitude doubles during reflection but the pulse recovers to the original shape in the 12th time steps and continues to propagate toward the free boundary. Reflection from the free boundary results in tensile moment pulse of the same shape as original incident compressive moment pulse that continues to propagate toward the impermeable boundary at $x=0$.

Figure 3(b) shows the propagation, reflection and propagation upon reflection of the same compressive ${}_s m_{11}$ pulse as in **Figure 3(a)** but in the presence of dissipation. We choose dimensionless dissipation coefficient $c_d^*=0.002$. From **Figure 3(b)** we observe almost the same behavior of the moment pulse as that of ${}_s^d\sigma_{11}$ pulse in **Figure 2(b)**. Presence of dissipation resulting in continued amplitude decay and base elongation during the propagation. Amplitude decay is more pronounced for the incident pulse and the base elongation is more significant in the reflected pulse.

Rotational Wave: Model RW2

In this study, we consider mathematical model RW3, Equation (43). In this mathematical model rotational wave speed is $\sqrt{\alpha_1^*}$ and the dissipation is controlled by the dimensionless dissipation coefficient c_d^*. We apply a moment (${}_s m_{11}$) pulse of duration $2\Delta t$ at the boundary $x=L=1$.

In the first study, we choose $\Delta t=0.1$, $\alpha_1^*=2.25$ and $c_d^*=0$ (undamped case). The wave speed is $\sqrt{2.25}=1.5$, thus the pulse would reach $x=0$

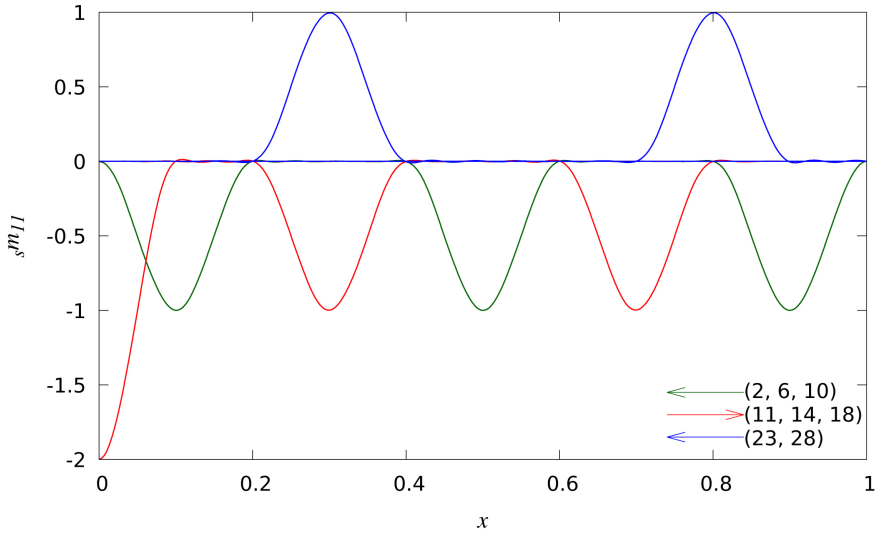

(a) Undamped case ($c_d^* = 0$)

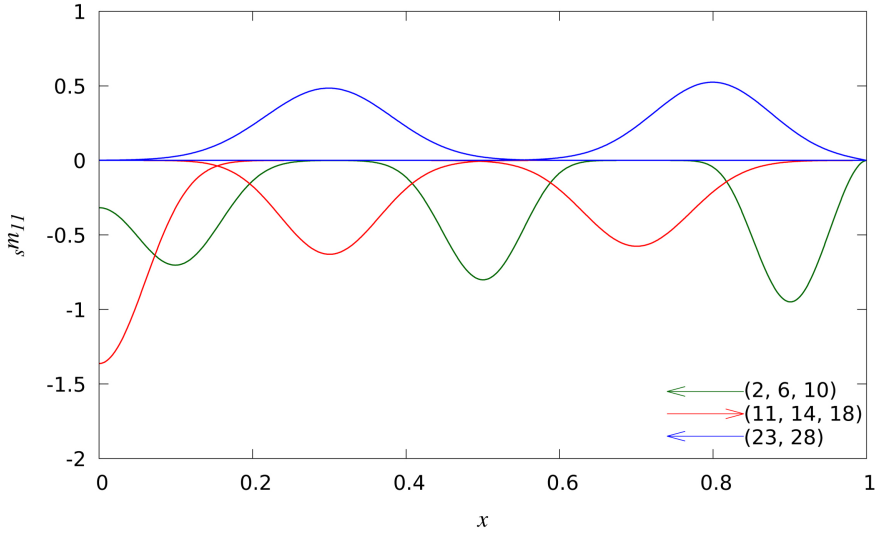

(b) Damped case ($c_d^* = 0.002$)

Figure 3. Evolution of Cauchy Moment wave: $_s m_{11}$ versus position x (Model RW1).

boundary in $(1/1.5)/0.1 = 6.67$ time steps. **Figure 4(a)** show propagation and reflection of the moment pulse. **Figure 4(b)** show propagation and reflection of the moment pulse for $\alpha_1^* = 2.25$ *i.e.*, at the wave speed of 1.5 when $c_d^* = 0.002$. Diminished amplitudes and elongated base of the pulse is clearly observed during evolution. This is similar to RW1 ($c_d^* = 0.002$). In the next study, we apply the same moment pulse as in the previous study but choose $\alpha_1^* = 0.49$ and $c_d^* = 0$, hence rotational wave speed of $\sqrt{0.49} = 0.7$, thus the moment pulse will reach the boundary at $x = 0$ in $(1/0.7)/0.1 = 14.285$ time steps. **Figure 5(a)** and **Figure 5(b)** show propagation and reflection of the moment wave for $c_d^* = 0$ and $c_d^* = 0.002$. The undamped pulse ($c_d^* = 0$) maintains its base and amplitude during the entire evolution and when $c_d^* = 0.002$ progressive amplitude decay and base elongation of the pulse is observed for both values of α_1^*.

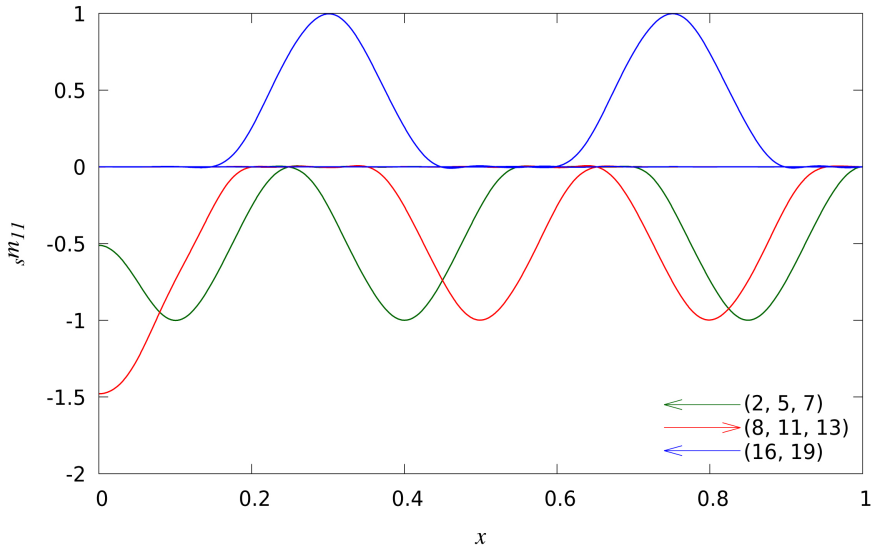

(a) Undamped case ($c_d^* = 0$)

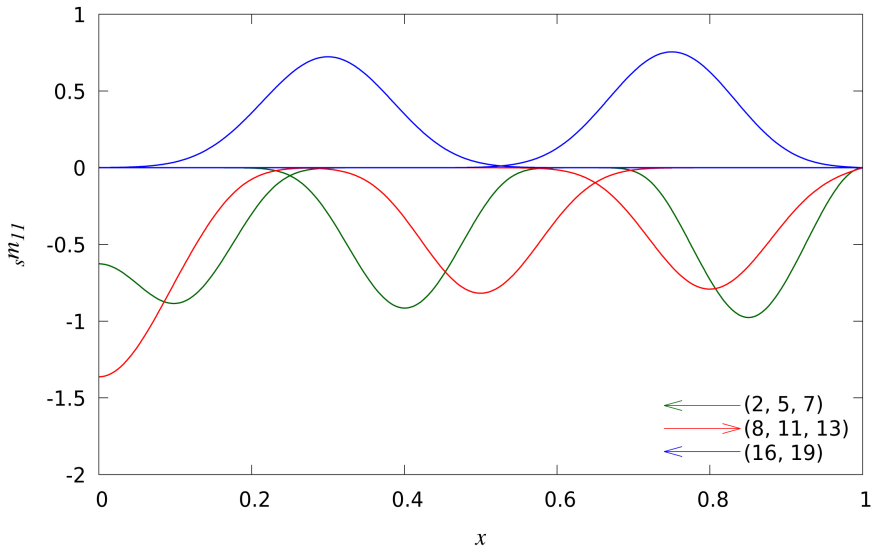

(b) Damped case ($c_d^* = 0.002$)

Figure 4. Evolution of Cauchy Moment wave: ${}_sm_{11}$ versus position x (Model RW2: $\alpha^* = 2.25$).

We remark that when the rotational wave speed is one, we are able to precisely locate the pulse at the impermeable boundary as the time to reach the impermeable boundary is integer multiple of Δt. In this case, we see perfect reflection of the ${}_sm_{11}$ pulse at the 11^{th} time step and the peak value of ${}_sm_{11}$ doubles, same as in the case of the translational stress wave. However, when rotational wave speed is not an integer multiple of Δt, precise arrival of ${}_sm_{11}$ pulse at $x = 0$ cannot be simulated as elapsed time is always an integer multiple of Δt. For this reason, we are not able to observe 2 (${}_sm_{11}$) in the peak values during the reflection process of the undamped case (**Figure 4(a)** and **Figure 5(a)**) when the rotational speed is not one.

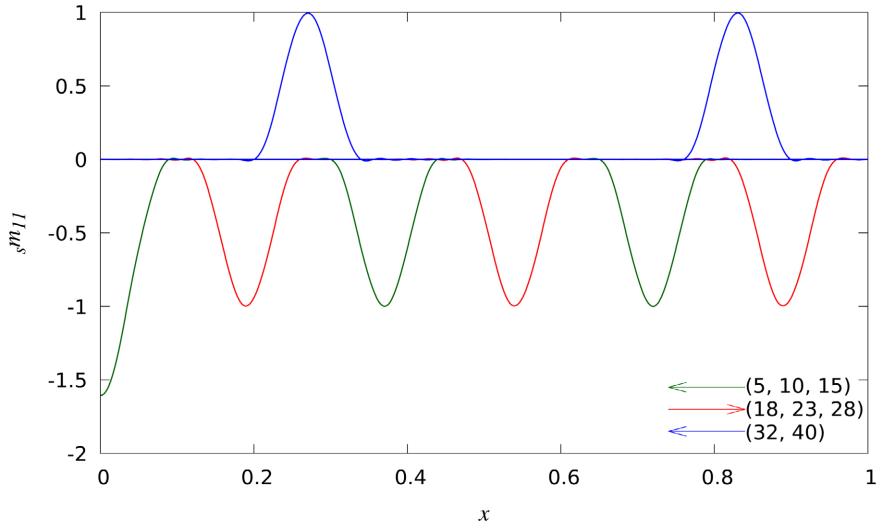

(a) Undamped case ($c_d^* = 0$)

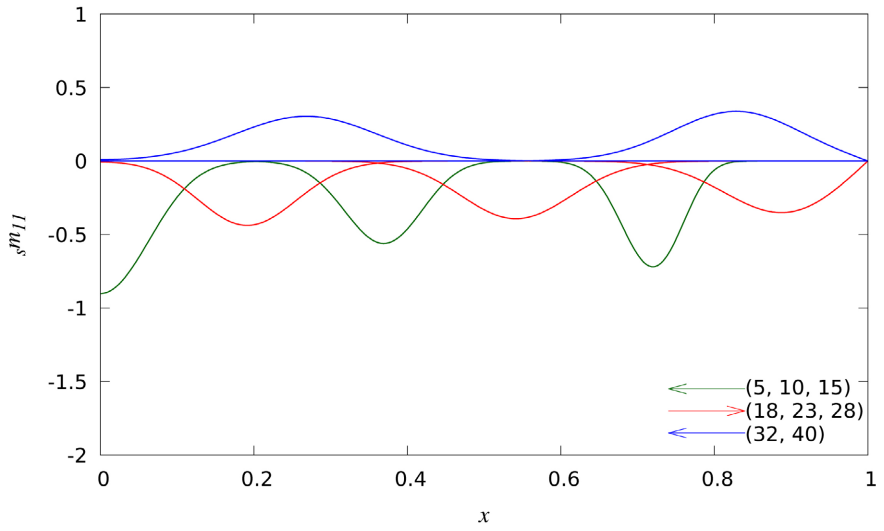

(b) Damped case ($c_d^* = 0.002$)

Figure 5. Evolution of Cauchy Moment wave: ${}_s m_{11}$ versus position x (Model RW2: $\alpha^* = 0.49$).

Remarks

1) In the model problem studies presented here the translational and rotational waves are decoupled. In $\mathbf{R}^2$ and $\mathbf{R}^3$ this may not be the case. Since the stress tensor is a function of $\left[{}_s^d J\right]$ and the moment tensor is a function of $\left[{}_a^d J\right]$, both stress and moment tensor waves are dependent on gradients of displacement. Thus, in $\mathbf{R}^2$ and $\mathbf{R}^3$ we expect interaction between the two waves. That is, as shown here, rotational waves depend upon $\hat{\alpha}_1$ and ${}^{\Theta}\overline{I}$ which in turn influences $\left[{}^d J\right]$, thus $\left[{}_s^d J\right]$, hence influencing translational waves. The model problem studies in $\mathbf{R}^2$ and $\mathbf{R}^3$ are needed to illustrate this physics.

2) The medium with and without microconstituents is always considered isotropic and homogeneous. Thus, in this micropolar theory there is absence of

wave dispersion in the micropolar medium as it is considered to be isotropic and homogeneous. This micropolar theory can only simulate wave propagation physics of translational and rotational waves and their interaction (when it exists) in $\mathbf{R}^2$ and $\mathbf{R}^3$ (future work).

3.2. Micropolar Viscous Fluids: Rotational Inertial Physics

Rotational wave?

The objective of the model problem studies presented in this section is to demonstrate the influence of rotational inertial physics in micropolar fluids in which NCCT is based on internal rotation rate physics. It is well known that in classical or micropolar viscous fluids, translational deviatoric stress waves can not exist due to the absence of elasticity. In this study, we only consider balance of angular momenta in 1D and associated constitutive theories to investigate the influence of rotational inertial physics.

Mathematical model: rotational wave?

The one dimensional form of BAM and the constitutive theory for the Cauchy moment tensor are given by (using $\bar{x}$ for $\bar{x}_1$).

$$ {}^{\Theta}\bar{I}\,\bar{\rho}\frac{\partial\left({}_i\bar{\omega}_1\right)}{\partial t}-\frac{\partial\left({}_s\bar{m}_{11}\right)}{\partial\bar{x}}=0 \tag{44}$$

$$ {}_s\bar{m}_{11}=\bar{\alpha}_1\left(\frac{1}{2}\frac{\partial\left({}_i\bar{\omega}_1\right)}{\partial\bar{x}}\right) \tag{45}$$

Substituting (45) in (44)

$$ {}^{\Theta}\bar{I}\,\bar{\rho}\frac{\partial\left({}_i\bar{\omega}_1\right)}{\partial t}-\frac{\bar{\alpha}_1}{2}\left(\frac{\partial^2\left({}_i\bar{\omega}_1\right)}{\partial\bar{x}^2}\right)=0 \tag{46}$$

Remarks

1) We clearly see that this Equation (46) will not permit a moment $({}_s\bar{m}_{11})$ wave as it is not a wave equation due to the absence of $\frac{\partial^2\left({}_i\bar{\omega}_1\right)}{\partial t^2}$ in place of $\frac{\partial\left({}_i\bar{\omega}_1\right)}{\partial t}$.

2) However it is interesting to study its solution for varying ${}^{\Theta}\bar{I}$ values.

Dimensionless form of the mathematical model

Recasting (46) with hat $(\wedge)$ on all quantities indicating that they have their usual dimensions (or units)

$$ {}^{\Theta}\hat{\bar{I}}\,\hat{\bar{\rho}}\frac{\partial\left({}_i\hat{\bar{\omega}}_1\right)}{\partial\hat{t}}-\frac{\hat{\bar{\alpha}}_1}{2}\left(\frac{\partial^2\left({}_i\hat{\bar{\omega}}_1\right)}{\partial\hat{\bar{x}}^2}\right)=0 \tag{47}$$

and using

$$\left.\begin{aligned} &{}^{\Theta}\bar{I}={}^{\Theta}\hat{\bar{I}}/{}^{\Theta}I_0,\quad \bar{\rho}=\hat{\bar{\rho}}/\rho_0,\quad \bar{x}=\hat{\bar{x}}/L_0\\ &{}_i\bar{\omega}_1={}_i\hat{\bar{\omega}}_1/\omega_0,\quad t_0=L_0/\omega_0,\\ &\text{and}\quad \omega_0=\sqrt{(\alpha_1)_0/{}^{\Theta}I_0\rho_0},\quad \bar{\alpha}_1=\hat{\bar{\alpha}}_1/(\alpha_1)_0 \end{aligned}\right\} \tag{48}$$

We can write (47) as

$$ {}^{\Theta}\bar{I}\,\bar{\rho}\frac{\partial\left({}_{i}\bar{\omega}_1\right)}{\partial t}-\left(\frac{\bar{\alpha}_1}{2}\right)\frac{\left(\alpha_1\right)_0}{L_0\,{}^{\Theta}I_0\rho_0}\left(\frac{\partial^2\left({}_{i}\bar{\omega}_1\right)}{\partial\bar{x}^2}\right)=0 \tag{49} $$

If we choose ${}^{\Theta}I_0={}^{\Theta}\hat{\bar{I}}$, $\rho_0=\hat{\bar{\rho}}$ and $\left(\alpha_1\right)_0=\hat{\bar{\alpha}}_1$ then (49) can be reduced to

$$ \frac{\partial\left({}_{i}\bar{\omega}_1\right)}{\partial t}-\bar{c}_2\left(\frac{\partial^2\left({}_{i}\bar{\omega}_1\right)}{\partial\bar{x}^2}\right)=0 \tag{50} $$

in which $\bar{c}_2=\left(\hat{\bar{\alpha}}_1\right)\Big/\left(2L_0\,{}^{\Theta}\hat{\bar{I}}\hat{\bar{\rho}}\right)$, dimensionless dissipation coefficient. PDE (50) can be cast as a system of two first order PDEs by using moment ${}_{s}\bar{m}_{11}$ as auxiliary variable and we have

$$ \left.\begin{aligned}&\frac{\partial\left({}_{i}\bar{\omega}_1\right)}{\partial t}-\frac{\partial\left({}_{s}\bar{m}_{11}\right)}{\partial\bar{x}}=0\\&{}_{s}\bar{m}_{11}=\bar{c}_2\frac{\partial\left({}_{i}\bar{\omega}_1\right)}{\partial\bar{x}}\end{aligned}\right\} \tag{51} $$

PDEs in (51) are helpful in defining BCs and ICs, hence are used in the computations.

Numerical Studies

Rotational wave?

We consider mathematical model (50) or (51). It is evident (50) is not a wave equation as a wave equation must have second order spatial and second order time derivatives of the dependent variable. Thus, (50) can not describe a wave, which is not a surprise, because classical as well as micropolar fluids do not possess elasticity, hence do not have stiffness, thus they cannot support deviatoric Cauchy stress wave or Cauchy moment wave.

Equation (50) is in fact a time dependent diffusion equation in which $\bar{c}_2\propto\frac{1}{{}^{\Theta}\bar{I}}$ is the diffusion coefficient. Thus low values of ${}^{\Theta}\bar{I}$ correspond to high values of $\bar{c}_2$ and vice versa. Details of the schematic, space-time strips and discretization of a space-time strip remain the same as shown in **Figure 1**. We apply a negative ${}_{s}\bar{m}_{11}$ moment pulse of duration $2\Delta t$ on the boundary at $\bar{x}=1$ such that ${}_{s}\bar{m}_{11}\in[0,-1]\ \ \forall t\in[0,\Delta t]$; ${}_{s}\bar{m}_{11}\in[-1,0]\ \ \forall t\in[\Delta t,2\Delta t]$ and ${}_{s}\bar{m}_{11}=0$ for $t\geq 2\Delta t$ (similar to BC shown in **Figure 1(e)**). We choose a discretization of 30 nine node p-version hierarchical space-time elements with p-levels of nine in space and time. Evolution is computed for 30 time steps using $\Delta t=0.1$ with local approximation of class C^1 in space and time, We choose two values of $\bar{c}_2=0.0001,0.001$. Evolutions for different values of time for the two choices of $\bar{c}_2$ are shown in **Figure 6(a)** and **Figure 6(b)**. For both values of $\bar{c}_2$, the applied pulse progressively diffuses as time elapses. We observe significantly high diffusion of the applied moment pulse for $\bar{c}_2=0.001$ compared to $\bar{c}_2=0.0001$ as expected. We clearly observe lack of existence and propagation of rotational or moment waves due to lack of elasticity, demonstrating that rotational waves can not exist in micropolar fluids with rotational inertial physics.

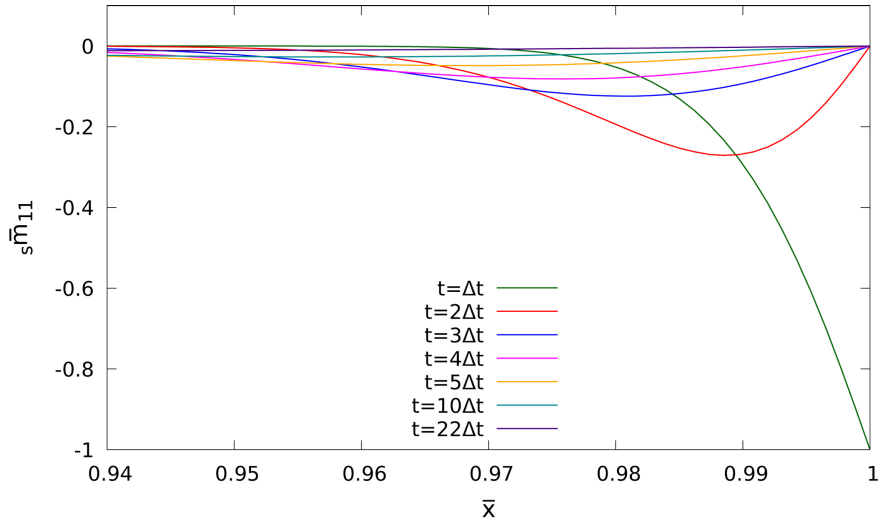

(a) ${}_s\bar{m}_{11}$ versus $\bar{x}$ ($\bar{c}_2 = 0.001$)

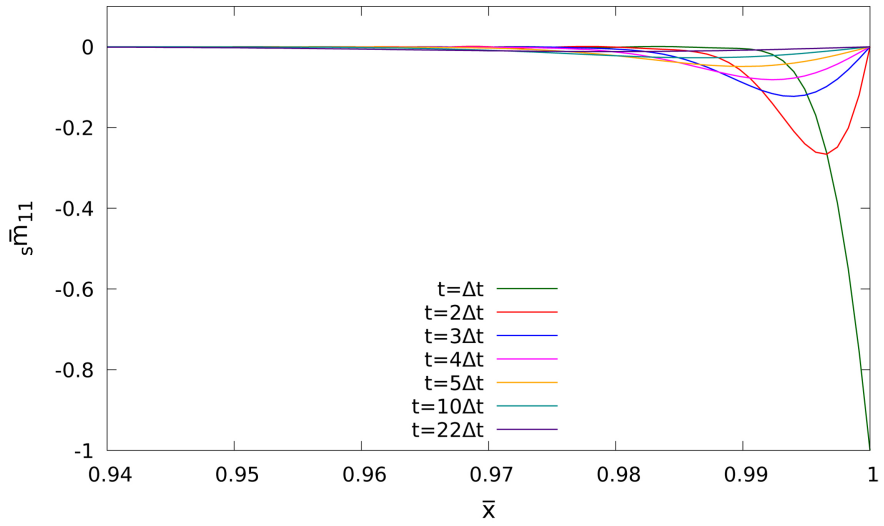

(b) ${}_s\bar{m}_{11}$ versus $\bar{x}$ ($\bar{c}_2 = 0.0001$)

Figure 6. Cauchy Moment ${}_s\bar{m}_{11}$ versus position $\bar{x}$.

3.2.1. Developing Pressure Driven Flow between Parallel Plates and Developing Couette Flow

In this study, we consider developing pressure driven flow between parallel plates and developing Couette flow in which the mathematical models are based on: CCM, NCCM without rotational inertial physics and NCCM with rotational inertial physics. Only the micropolar nonclassical continuum theory based on internal rotation rates is considered [4]. **Figure 7** shows a schematic of the dimensionless configuration of parallel plates.

Away from the ends A and B, the physics of the flow is purely one dimensional (in the $\bar{y}$ direction) velocity $\bar{u}$ is a dependent variable, velocity $\bar{v}$ in the $\bar{y}$ direction is zero regardless of the type of mathematical model hence, Cauchy shear stress is the only non-zero stress (details are given in the following). We present details of three mathematical models (as mentioned above): based

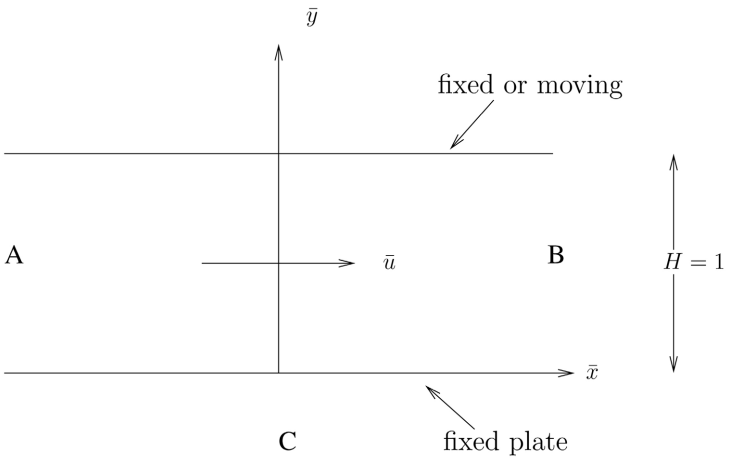

Figure 7. Spatial domain for pressure driven and Couette flow.

on CCM, NCCM without rotational inertial physics and NCCM with rotational inertial physics. We nondimensionalize these mathematical models using the following reference quantities and dimensionless quantities.

$$\left.\begin{aligned}
&\bar{x}=\hat{\bar{x}}/L_0,\quad \bar{y}=\hat{\bar{y}}/L_0,\quad \bar{\eta}=\hat{\bar{\eta}}/\eta_0,\quad \bar{\alpha}=\hat{\bar{\alpha}}/\alpha_0\\
&\bar{m}_{23}^{(0)}=\hat{\bar{m}}_{23}^{(0)}/m_0,\quad {}^{d}_{s}\bar{\sigma}_{21}^{(0)}={}^{d}_{s}\hat{\bar{\sigma}}_{21}^{(0)}/\tau_0,\quad {}_{a}\bar{\sigma}_{21}^{(0)}={}_{a}\hat{\bar{\sigma}}_{21}^{(0)}/\tau_0\\
&m_0=\tau_0 L_0,\quad \tau_0=\rho_0 v_0^2=p_0\left(\text{characteristic kinetic energy}\right)\\
&\bar{u}=\hat{\bar{u}}/v_0,\quad \bar{v}=\hat{\bar{v}}/v_0,\quad t_0=L_0/v_0\\
&{}_{i}\bar{\omega}_3={}_{i}\hat{\bar{\omega}}_3/\omega_0,\quad \omega_0=t_0,\quad {}^{\Theta}\bar{I}={}^{\Theta}\hat{\bar{I}}/{}^{\Theta}I_0
\end{aligned}\right\}\tag{52}$$

Mathematical model based on CCM: Model A

Balance of linear momenta in the $\bar{x}$ direction and the constitutive theory for deviatoric Cauchy stress ${}_{d}\bar{\sigma}_{12}^{(0)}={}_{d}\bar{\sigma}_{21}^{(0)}$ are the only two equations needed in this case and are given in the following (with usual dimensions for all quantities) for incompressible classical fluid.

$$\left.\begin{aligned}
&\hat{\bar{\rho}}\frac{\partial\hat{\bar{u}}}{\partial\hat{t}}+\frac{\partial\hat{\bar{p}}}{\partial\hat{\bar{x}}}-\frac{\partial\left({}^{d}_{s}\hat{\bar{\sigma}}_{21}^{(0)}\right)}{\partial\hat{\bar{y}}}=0\\
&{}^{d}_{s}\hat{\bar{\sigma}}_{21}^{(0)}=\hat{\bar{\eta}}\frac{\partial\hat{\bar{u}}}{\partial\hat{\bar{y}}}
\end{aligned}\right\}\tag{53}$$

We can nondimensionalize (53) using (52) and if we choose $\rho_0=\hat{\bar{\rho}}$, $\eta_0=\hat{\bar{\eta}}$, then the dimensionless form of (53) can be written as

$$\left.\begin{aligned}
&\frac{\partial\bar{u}}{\partial t}+\frac{\partial\bar{p}}{\partial\bar{x}}-\frac{\partial\left({}^{d}_{s}\bar{\sigma}_{21}^{(0)}\right)}{\partial\bar{y}}=0\\
&{}^{d}_{s}\bar{\sigma}_{21}^{(0)}=\frac{1}{Re}\frac{\partial\bar{u}}{\partial\bar{y}}
\end{aligned}\right\}\tag{54}$$

In case of pressure driven flow, $\frac{\partial\bar{p}}{\partial\bar{x}}$ is given. For non-pressure driven Couette flow, $\frac{\partial\bar{p}}{\partial\bar{x}}=0$. In (54), Re is Reynolds number and is given by (based on

reference quantities) $Re = \dfrac{L_0 \rho_0 v_0}{\eta_0}$. Equation (54) is a first order system of two PDEs in two dependent variables $\bar{u}$ and ${}^{d}_{s}\bar{\sigma}^{(0)}_{21}$. In this case, flow characteristics depend upon dimensionless parameter *Re*.

Micropolar NCCT without rotational inertial physics: Model B

In this case, the mathematical model consists of BLM in $\bar{x}$ direction, balance of angular momenta about the $\bar{z}$ direction, constitutive theory for symmetric part of deviatoric Cauchy shear stress ${}^{d}_{s}\bar{\sigma}^{(0)}_{12} = {}^{d}_{s}\bar{\sigma}^{(0)}_{21}$, constitutive theory for symmetric Cauchy moment ${}_{s}\bar{m}_{23}$ and definition of angular rotation rate ${}_{i}\bar{\omega}_3$ *i.e.*, rotation rate about $\bar{z}$. We can write the following (with their usual dimensions) using the CBL and the constitutive theories given for $\mathbb{R}^3$ by Equations (11)-(22), in the absence of body forces and body moments.

$$\left.\begin{aligned}
&\hat{\rho}\frac{\partial \hat{u}}{\partial \hat{t}} + \frac{\partial \hat{p}}{\partial \hat{x}} - \frac{\partial\left({}^{d}_{s}\hat{\bar{\sigma}}^{(0)}_{21}\right)}{\partial \hat{y}} - \frac{\partial\left({}^{d}_{a}\hat{\bar{\sigma}}^{(0)}_{21}\right)}{\partial \hat{y}} = 0\\
&\frac{\partial\left({}_{s}\hat{\bar{m}}^{(0)}_{23}\right)}{\partial \hat{y}} + 2\left({}^{d}_{a}\hat{\bar{\sigma}}^{(0)}_{21}\right) = 0\\
&{}^{d}_{s}\hat{\bar{\sigma}}^{(0)}_{12} = {}^{d}_{s}\hat{\bar{\sigma}}^{(0)}_{21} = \hat{\bar{\eta}}\frac{\partial \hat{\bar{u}}}{\partial \hat{\bar{y}}}\\
&{}_{s}\hat{\bar{m}}^{(0)}_{23} = \frac{\hat{\bar{\alpha}}}{2}\frac{\partial\left({}_{i}\hat{\bar{\omega}}_3\right)}{\partial \bar{y}}\\
&{}_{i}\hat{\bar{\omega}}_3 = -\frac{1}{2}\frac{\partial \hat{\bar{u}}}{\partial \hat{\bar{y}}}
\end{aligned}\right\} \tag{55}$$

We can nondimensionalize (55) using (52), and if we choose ${}^{\Theta}I_0 = {}^{\Theta}\hat{\bar{I}}$, $\rho_0 = \hat{\bar{\rho}}$, $\eta_0 = \hat{\bar{\eta}}$, then (55) can be written as

$$\left.\begin{aligned}
&\bar{\rho}\frac{\partial \bar{u}}{\partial t} + \frac{\partial \bar{p}}{\partial \bar{x}} - \frac{\partial\left({}^{d}_{s}\bar{\sigma}^{(0)}_{21}\right)}{\partial \bar{y}} - \frac{\partial\left({}^{d}_{a}\bar{\sigma}^{(0)}_{21}\right)}{\partial \bar{y}} = 0\\
&\frac{\partial\left({}_{s}\bar{m}^{(0)}_{23}\right)}{\partial \bar{y}} + 2\left({}^{d}_{a}\bar{\sigma}^{(0)}_{21}\right) = 0\\
&{}^{d}_{s}\bar{\sigma}^{(0)}_{12} = {}^{d}_{s}\bar{\sigma}^{(0)}_{21} = \frac{1}{Re}\frac{\partial \bar{u}}{\partial \bar{y}}\\
&{}_{s}\bar{m}^{(0)}_{23} = \frac{\bar{\alpha}}{2}\frac{\partial\left({}_{i}\bar{\omega}_3\right)}{\partial \bar{y}}\\
&{}_{i}\bar{\omega}_3 = -\frac{1}{2}\frac{\partial \bar{u}}{\partial \bar{y}}
\end{aligned}\right\} \tag{56}$$

in which $\bar{\alpha} = \hat{\bar{\alpha}} / \tau_0 L_0^2 t_0$, dimensionless material coefficient for micropolar nonclassical physics. Equations (56) is a system of five first order PDEs in five dependent variables: $\bar{u}$, ${}^{d}_{s}\bar{\sigma}^{(0)}_{21}$, ${}^{d}_{a}\bar{\sigma}^{(0)}_{21}$, ${}_{s}\bar{m}^{(0)}_{23}$ and ${}_{i}\bar{\omega}_3$.

Dimensionless parameters *Re* and $\bar{\alpha}$ control classical physics and micropolar nonclassical physics.

Micropolar NCCT with rotational inertial physics: Model C

The mathematical model consists of BLM in $\bar{x}$ direction, BAM about $\bar{z}$

direction, BMM balance law, constitutive theory for symmetric part of the deviatoric Cauchy shear stress ${}^{d}_{s}\bar{\sigma}^{(0)}_{12} = {}^{d}_{s}\bar{\sigma}^{(0)}_{21}$, constitutive theory for symmetric Cauchy moment ${}_{s}\bar{m}^{(0)}_{23}$, definition of angular rotation rate ${}_{i}\bar{\omega}_{3}$ and the constraint equations resulting from the entropy inequality.

Using the mathematical model in $\mathbb{R}^3$ (Equations (11)-(22)) and noting that in this case $\bar{v}=0$, $\bar{w}=0$, we can write the following for CBL and constitutive theories (in the absence of body forces and body moments) and the constraint equation

$$\left.\begin{aligned}
&\hat{\bar{\rho}}\frac{\partial\hat{\bar{u}}}{\partial\hat{t}}+\frac{\partial\hat{\bar{p}}}{\partial\hat{\bar{x}}}-\frac{\partial\left({}^{d}_{s}\hat{\bar{\sigma}}^{(0)}_{21}\right)}{\partial\hat{\bar{y}}}-\frac{\partial\left({}^{d}_{a}\hat{\bar{\sigma}}^{(0)}_{21}\right)}{\partial\hat{\bar{y}}}=0\\
&\hat{\bar{\rho}}\left({}^{\Theta}\hat{\bar{I}}\right)\left(\frac{\partial\left({}_{i}\hat{\bar{\omega}}_{3}\right)}{\partial\hat{t}}\right)-\frac{\partial\left({}_{s}\hat{\bar{m}}^{(0)}_{23}\right)}{\partial\hat{\bar{y}}}-\frac{\partial\left({}_{a}\hat{\bar{m}}^{(0)}_{23}\right)}{\partial\hat{\bar{y}}}+2\left({}^{d}_{a}\hat{\bar{\sigma}}^{(0)}_{21}\right)=0\\
&{}^{d}_{s}\hat{\bar{\sigma}}^{(0)}_{12}={}^{d}_{s}\hat{\bar{\sigma}}^{(0)}_{21}=\hat{\bar{\eta}}\frac{\partial\hat{\bar{u}}}{\partial\hat{\bar{y}}}\\
&{}_{s}\hat{\bar{m}}^{(0)}_{23}=\frac{\hat{\bar{\alpha}}}{2}\frac{\partial\left({}_{i}\hat{\bar{\omega}}_{3}\right)}{\partial\bar{y}}\\
&{}_{i}\hat{\bar{\omega}}_{3}=-\frac{1}{2}\frac{\partial\hat{\bar{u}}}{\partial\hat{\bar{y}}}
\end{aligned}\right\}\tag{57}$$

$${}^{\Theta}\hat{\bar{I}}\hat{\bar{v}}\left({}_{i}\hat{\bar{\omega}}_{3}\right)-{}_{s}\hat{\bar{m}}^{(0)}_{23}-{}_{a}\hat{\bar{m}}^{(0)}_{23}=0\quad\text{(BMM when }\bar{v}\neq 0\text{)}\tag{58}$$

$${}_{s}\hat{\bar{m}}^{(0)}_{23}\left({}_{i}\hat{\bar{\omega}}_{3}\right)=0\quad\text{(constraint equation)}\tag{59}$$

When $\bar{v}=0$ (which is the case here), BMM (58) reduces to

$${}_{s}\hat{\bar{m}}_{23}+{}_{a}\hat{\bar{m}}_{23}=0\tag{60}$$

Equation (60) suggests that ${}_{a}\hat{\bar{m}}^{(0)}_{23}=-{}_{s}\hat{\bar{m}}^{(0)}_{23}$ or the nonsymmetric moment tensor $\hat{\bar{m}}^{(0)}_{23}$ is zero, implying no micropolar physics. This of course is erroneous, hence in this case (60) cannot be used as part of the mathematical model. The constraint Equation (59) implies that either ${}_{s}\hat{\bar{m}}^{(0)}_{23}=0$ or ${}_{i}\hat{\bar{\omega}}_{3}=0$ for all $\bar{x},t\in\bar{\Omega}_{xt}$. This also is erroneous, thus (58) and (59) cannot be considered as a part of the mathematical model, thus Equation (57) constitutes the mathematical model. We can nondimensionalize (57) using (52), and if we choose ${}^{\Theta}I_0={}^{\Theta}\hat{\bar{I}}$, $\rho_0=\hat{\bar{\rho}}$, $\eta_0=\hat{\bar{\eta}}$, then we can obtain the following from (57).

$$\left.\begin{aligned}
&\bar{\rho}\frac{\partial\bar{u}}{\partial t}+\frac{\partial\bar{p}}{\partial\bar{x}}-\frac{\partial\left({}^{d}_{s}\bar{\sigma}^{(0)}_{21}\right)}{\partial\bar{y}}-\frac{\partial\left({}^{d}_{a}\bar{\sigma}^{(0)}_{21}\right)}{\partial\bar{y}}=0\\
&\bar{\beta}\frac{\partial\left({}_{i}\bar{\omega}_{3}\right)}{\partial t}-\frac{\partial\left({}_{s}\bar{m}^{(0)}_{23}\right)}{\partial\bar{y}}+2\left({}^{d}_{a}\bar{\sigma}^{(0)}_{21}\right)=0\\
&{}^{d}_{s}\bar{\sigma}^{(0)}_{12}={}^{d}_{s}\bar{\sigma}^{(0)}_{21}=\frac{1}{Re}\frac{\partial\bar{u}}{\partial\bar{y}}\\
&{}_{s}\bar{m}^{(0)}_{23}=\frac{\bar{\alpha}}{2}\frac{\partial\left({}_{i}\bar{\omega}_{3}\right)}{\partial\bar{y}}\\
&{}_{i}\bar{\omega}_{3}=-\frac{1}{2}\frac{\partial\bar{u}}{\partial\bar{y}}
\end{aligned}\right\}\tag{61}$$

These are a system of five first order PDEs in five dependent variables: $\bar{u}$, ${}^{d}_{s}\bar{\sigma}^{(0)}_{21}$, ${}^{d}_{a}\bar{\sigma}^{(0)}_{21}$, ${}_{s}\bar{m}^{(0)}_{23}$ and ${}_{i}\bar{\omega}_{3}$. *Re*, $\bar{\alpha}$ and $\bar{\beta}$ control classical physics, non-classical physics without rotational inertial effects and nonclassical physics with rotational inertia effects, respectively. In (61), $\bar{\alpha}$ and $\bar{\beta}$ are defined as $\bar{\alpha} = \hat{\bar{\alpha}}/\tau_0 L_0^2 t_0$ and $\bar{\beta} = {}^{\Theta}I_0/L_0^2$.

Numerical studies

We consider two model problems in this section: developing flow between parallel plates and developing Couette flow. In both model problems, we compute solutions for Model A (CCM); Model B, NCCM with micropolar physics but absence of rotational inertial physics; and Model C, micropolar NCCM with rotational inertial physics. In Model A (CCM), the only dimensionless parameter is Re which controls the flow physics. In case of Model B, Re for CCM and $\bar{\alpha}$ for micropolar physics control the flow physics. In case of Model C, Re, $\bar{\alpha}_1$ and $\bar{\beta}_1$ all three control the physics. $\bar{\beta}_1$ is associated with rotational inertial physics. For both model problem studies we present evolutions for different combinations of $\bar{\alpha}$ and $\bar{\beta}$ for a fixed Re to illustrate their influence on flow physics. Computed solutions for Model B and C are always compared with Model A.

We recall that many works published by Surana *et al.* [8] [9] show that in micropolar NCCT presence of micro constituents offer resistance to flow *i.e.*, increasing value of $\bar{\alpha}$ results in diminishing flow rate. Material coefficient $\bar{\beta}$, due to rotational inertial physics, related to rotational inertial physics due to microconstituents is also expected provide further resistance to flow over and beyond $\bar{\alpha}$. In other words, we expect increasing $\bar{\alpha}$ as well as increasing $\bar{\beta}$ to provide increasing resistance to flow. Since the constitutive theories are not calibrated, we do not know actual values of $\bar{\alpha}$ and $\bar{\beta}$ for various fluids with varying microconstituents. In the model problem studies presented here, we choose $\bar{\alpha}$ and $\bar{\beta}$ such that we can demonstrate their relative influence on flow physics.

Developing flow between parallel plates

Figure 8 shows schematic, space-time strips and a uniform discretization of first space-time strip using 10 p-version hierarchical space-time finite elements. We consider solution of class C^{00} in space and time with p-level of nine in space and time, $Re = 100$ with $\Delta t = 1.0$. Flow is pressure driven with $\frac{\partial \bar{p}}{\partial \bar{x}} = -0.1$.

Case I

In the first study we choose

Model A (CCM), $Re = 100$

Model B (NCCM), $Re = 100$; $\bar{\alpha} = 0.0001, 0.001$.

Figures 9(a)-(d) show plots of the evolution of velocity $\bar{u}$ for $t = 5\Delta t$, $10\Delta t$, $20\Delta t$ and $40\Delta t$ for Models A and B. In case of Model A (CCM) the flow has no resistance due to microconstituents. In model B, with progressively increasing $\bar{\alpha}$ the flow resistance increases resulting in diminishing flow rate. This holds true for each value of time *t*. At $t = 40\Delta t$, we almost have stationary

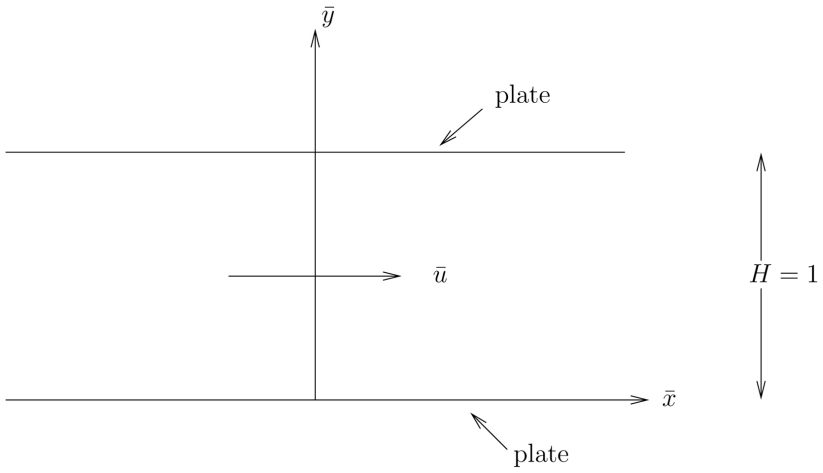

(a) Schematic of parallel plates

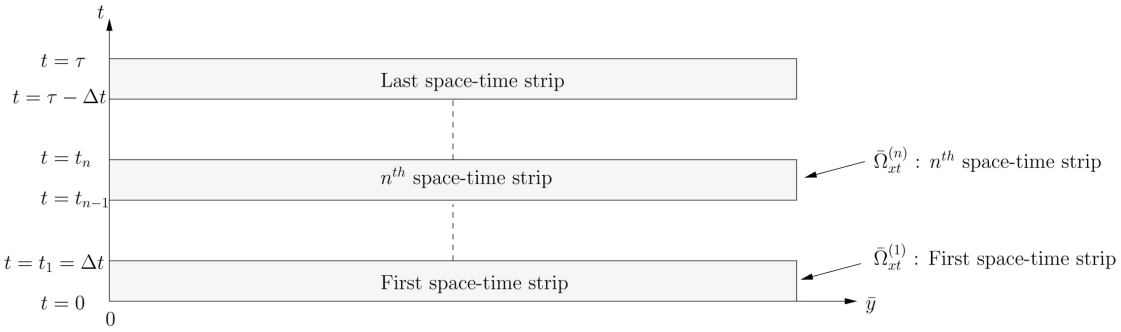

(b) Space-time strips

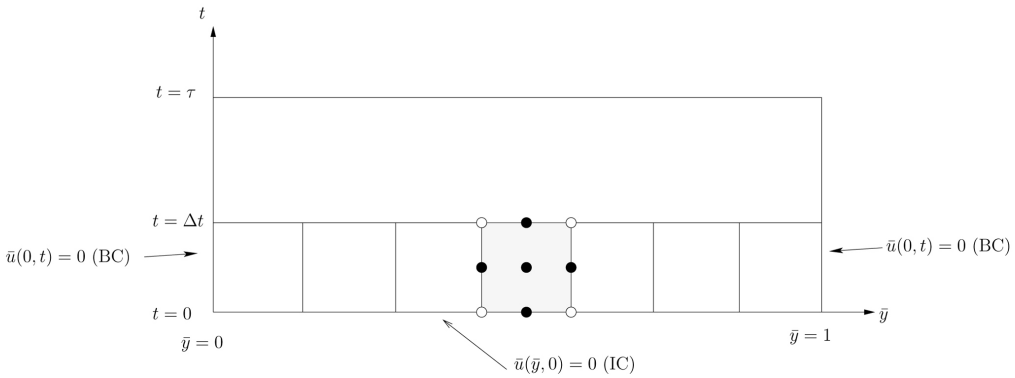

(c) Discretization $\left(\bar{\Omega}_{xt}^{(1)}\right)^T = \bigcup_e \bar{\Omega}_{xt}^{(e)}$ of the first space-time strip $\bar{\Omega}_{xt}^{(1)}$ and BCs, ICs

Figure 8. Developing flow between parallel plates, Discretization in time, Spatial discretization.

state of the developing flow. Significant reduction in flow rate with increasing $\bar{\alpha}$ is also obvious from the stationary state in **Figure 9(d)**. In CCM, rotation rates are a free field, hence they do not influence CCT. **Figure 10(a)** shows evolution of ${}_i\bar{\omega}_3$ versus $\bar{y}$ for Model A (CCM). At $t = 40\Delta t$, we almost have stationary sate at which $\frac{\partial\left({}_i\bar{\omega}_3\right)}{\partial\bar{y}} = constant$. Since ${}_i\bar{\omega}_3$ is a free field, ${}_s\bar{m}_{23} = 0$,

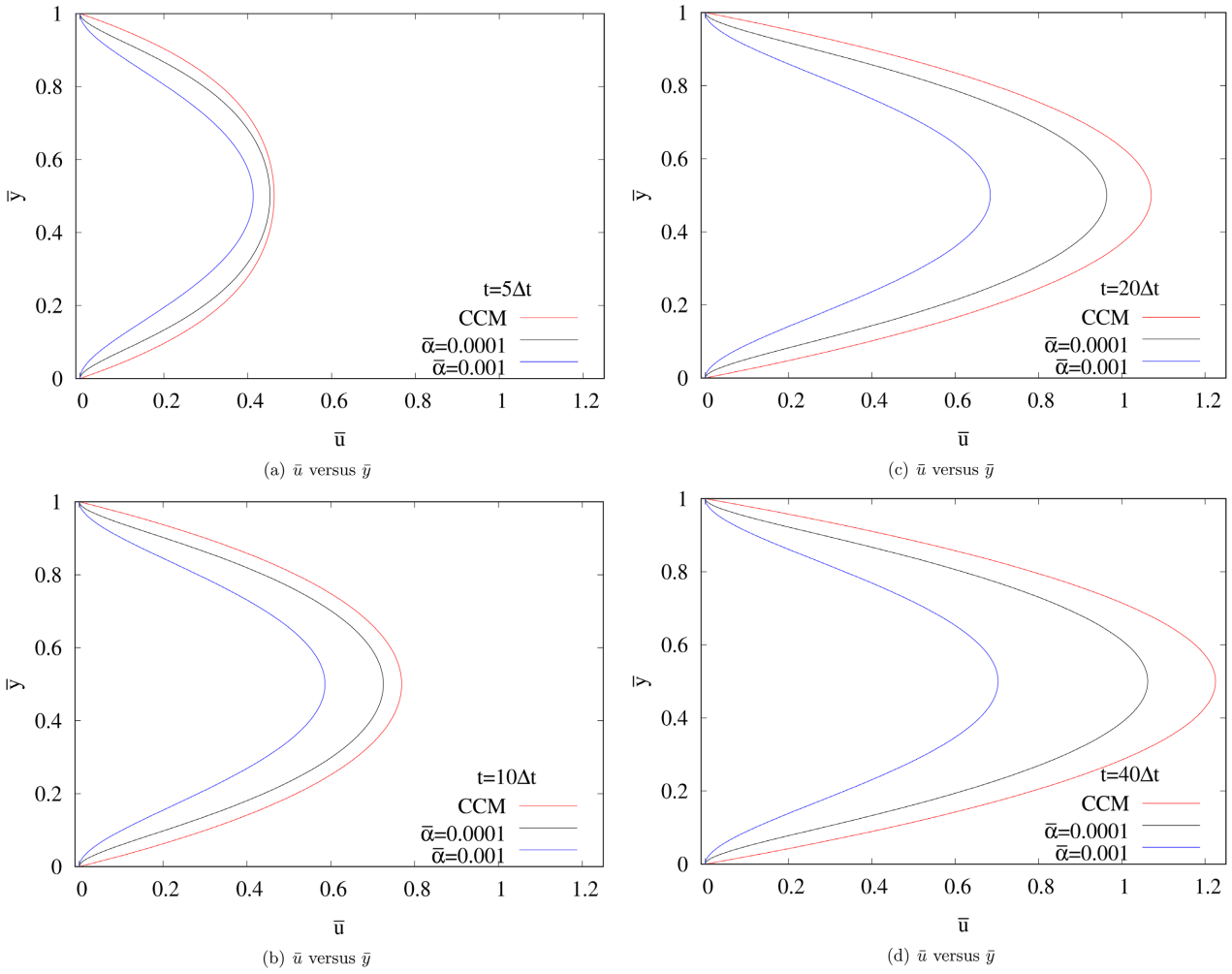

(a) $\bar{u}$ versus $\bar{y}$ (c) $\bar{u}$ versus $\bar{y}$

(b) $\bar{u}$ versus $\bar{y}$ (d) $\bar{u}$ versus $\bar{y}$

Figure 9. Developing flow between parallel plates: velocity $\bar{u}$ versus position $\bar{y}$: Models A and B (Case I).

shown in **Figure 10(b)**. **Figure 10(c)** and **Figure 10(d)** show evolution of ${}_i\bar{\omega}_3$ versus $\bar{y}$ and ${}_s\bar{m}_{23}$ versus $\bar{y}$ for Model B for $\bar{\alpha}=0.001$. Comparison of these evolutions with those in **Figure 10(a)** and **Figure 10(b)** clearly shows the influence of microconstituents on ${}_i\bar{\omega}_3$ and ${}_s\bar{m}_{23}$ as in this case ${}_i\bar{\omega}_3$ is not a free field, hence ${}_s\bar{m}_{23}$ is no longer zero.

Case II

In this study we consider the influence of both $\bar{\alpha}$ and $\bar{\beta}$ for fixed Reynolds number. We consider the following

Model A (CCM), $Re=100$ (same as in Case I)

Model C (NCCM with rotational inertial physics),

$Re=100$ (same as in Case I)

$$\left.\begin{matrix}\bar{\alpha}=0.0001\\ \bar{\alpha}=0.001\end{matrix}\right\}\bar{\beta}=0.05,0.9$$

Discretization, p-levels and other details remain the same as in case I. **Figures 11(a)-(d)** and **Figures 12(a)-(d)** show plots of velocity $\bar{u}$ versus $\bar{y}$ for $\bar{\alpha}=0.0001,0.001$, $\bar{\beta}=0.05$; and $\bar{\alpha}=0.0001,0.001$, $\bar{\beta}=0.9$. As we mentioned

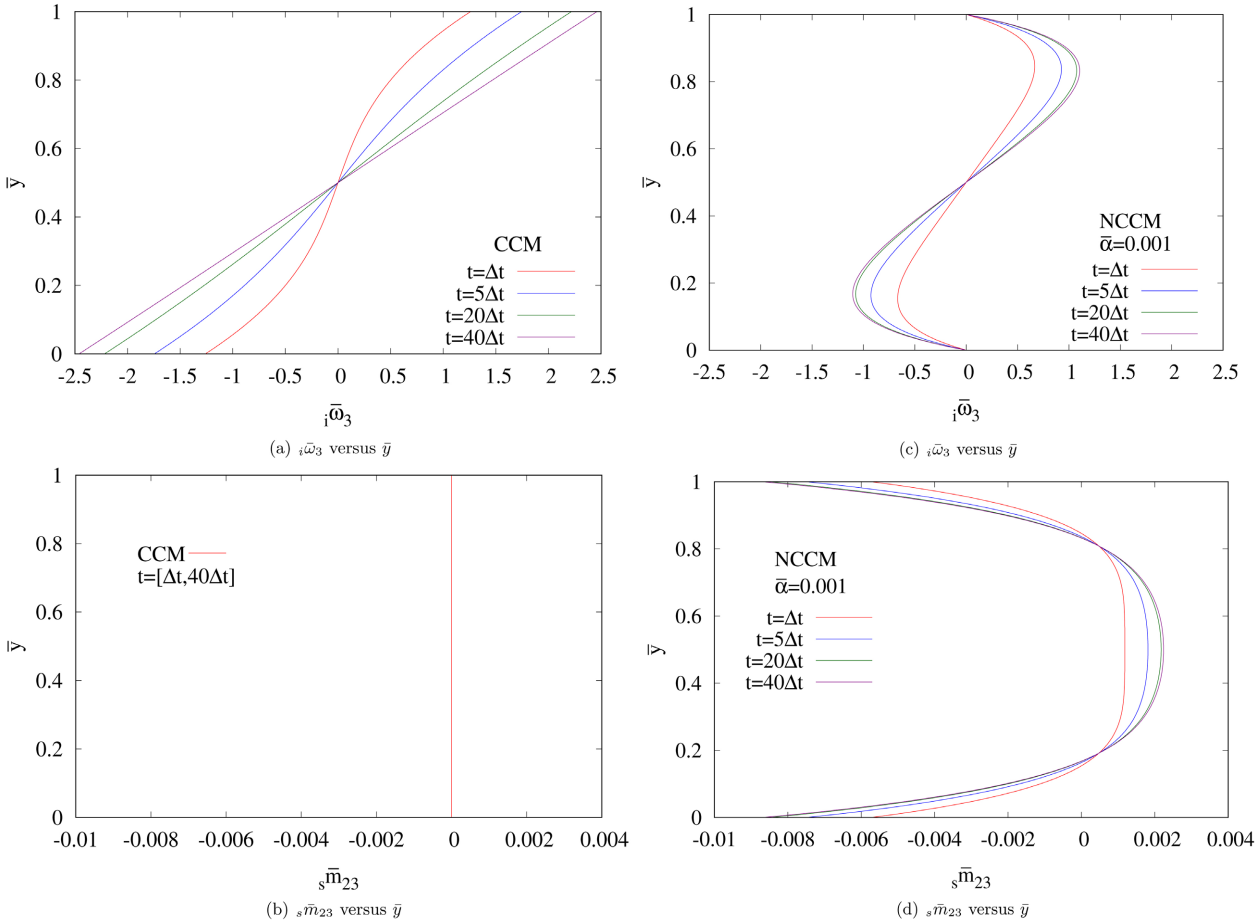

Figure 10. Developing flow between parallel plates: Model B: $_i\bar{\omega}_3$ versus $\bar{y}$ and $_s\bar{m}_{23}$ versus $\bar{y}$.

earlier both $\bar{\alpha}$ and $\bar{\beta}$ result in resistance to the flow but we expect that the degree of resistance is not the same for $\bar{\alpha}$ and $\bar{\beta}$ with similar change in their value. When comparing **Figures 11(a)-(d)** with **Figures 9(a)-(d)** we note that for same values of $\bar{\alpha}$ as in **Figures 9(a)-(d)** but with $\bar{\beta}=0$, we observe further reduction in the flow rate when $\bar{\beta}=0.05$. For $\bar{\beta}=0.9$ (**Figures 12(a)-(d)**) flow rate is further reduced compared to $\bar{\beta}=0.05$.

Case III

In this study we consider fixed $Re=100$, choose a fixed value of $\alpha=0.01$ and vary $\bar{\beta}$ to study evolution of velocity $\bar{u}$. We choose $\Delta t=1.0$ and $\bar{\beta}=0.05, 0.2$ and 0.5. Remaining details are same as in case I. **Figures 13(a)-(d)** show plots of $\bar{u}$ versus $\bar{y}$ for $t=5\Delta t$, $10\Delta t$, $20\Delta t$ and $40\Delta t$. At $t=40\Delta t$ we almost have stationary state of the flow. As expected, larger values of $\bar{\beta}$ offer more resistance to flow and requires more time to reach stationary state and vice versa. We note that stationary state is same for all $\bar{\beta}$ values. **Figure 14(a)** and **Figure 14(b)** show evolution of $_i\bar{\omega}_3$ versus $\bar{y}$ and $_s\bar{m}_{23}$ versus $\bar{y}$ (case II) for $Re=100$, $\bar{\alpha}=0.001$ and $\bar{\beta}=0.9$. Comparing this with **Figure 10(c)** and **Figure 10(d)** ($\bar{\alpha}=0.001$, $\bar{\beta}=0.0$), we clearly note reduced values of $_i\bar{\omega}_3$ during the evolution for $\bar{\beta}=0.9$ in **Figure 14(a)**,

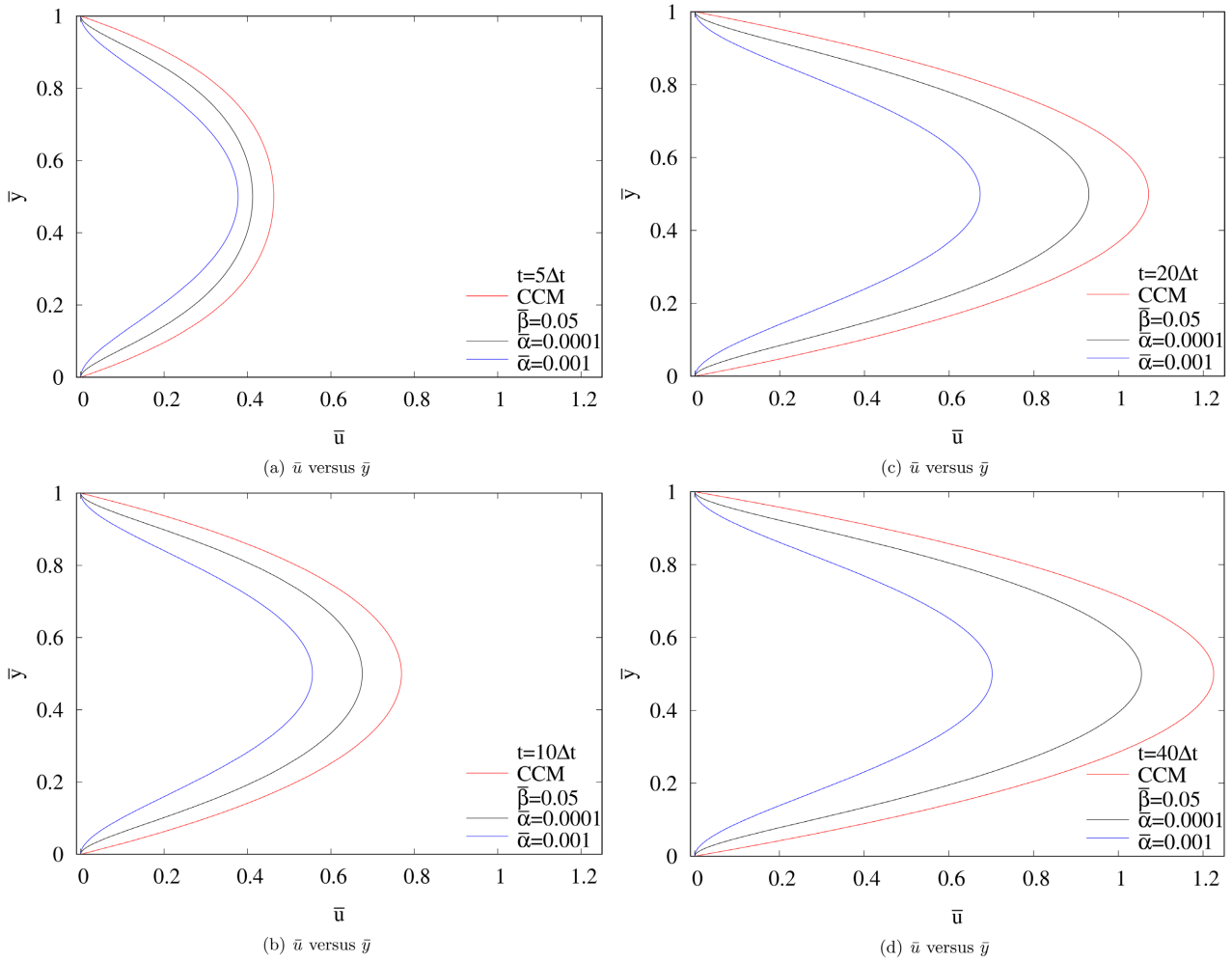

(a) $\bar{u}$ versus $\bar{y}$ (c) $\bar{u}$ versus $\bar{y}$

(b) $\bar{u}$ versus $\bar{y}$ (d) $\bar{u}$ versus $\bar{y}$

Figure 11. Developing flow between parallel plates: velocity $\bar{u}$ versus position $\bar{y}$: Models A and C (Case II), $\bar{\beta}=0.05$.

Cauchy moment ${}_s\bar{m}_{23}$ adjusts accordingly. This of course is due to increased resistance to flow due to $\bar{\beta}$.

Developing Couette flow

The configuration of parallel plates and other details remain the same as in **Figure 8**. We choose $Re=5$ in all studies. A 10 element uniform mesh with p-levels of nine in space and time and a solution of class C^{00} with $\Delta t=0.01$ is considered. At the top plate ($\bar{y}=1.0$) a velocity of 1.0 is applied over Δt in a continuous and differentiable manner *i.e.*, $\bar{u}\in[0,1]$ $\forall t\in[0,\Delta t]$ and $u=1.0$ $\forall t\geq\Delta t$.

Case A

Model A (CCM): $Re=5$

Model B (NCCM): $Re=5$; $\bar{\alpha}=0.0001,0.001$

Figures 15(a)-(c) show evolution of $\bar{u}$ versus $\bar{y}$ at $t=2\Delta t$, $5\Delta t$ and $10\Delta t$. For each value of time the velocity $\bar{u}$ for both $\bar{\alpha}$ values is lower than from Model A (CCM) as expected. Furthermore, higher values of $\bar{\alpha}$ yield lower values of velocity $\bar{u}$ compared to lower values of $\bar{\alpha}$ during the entire

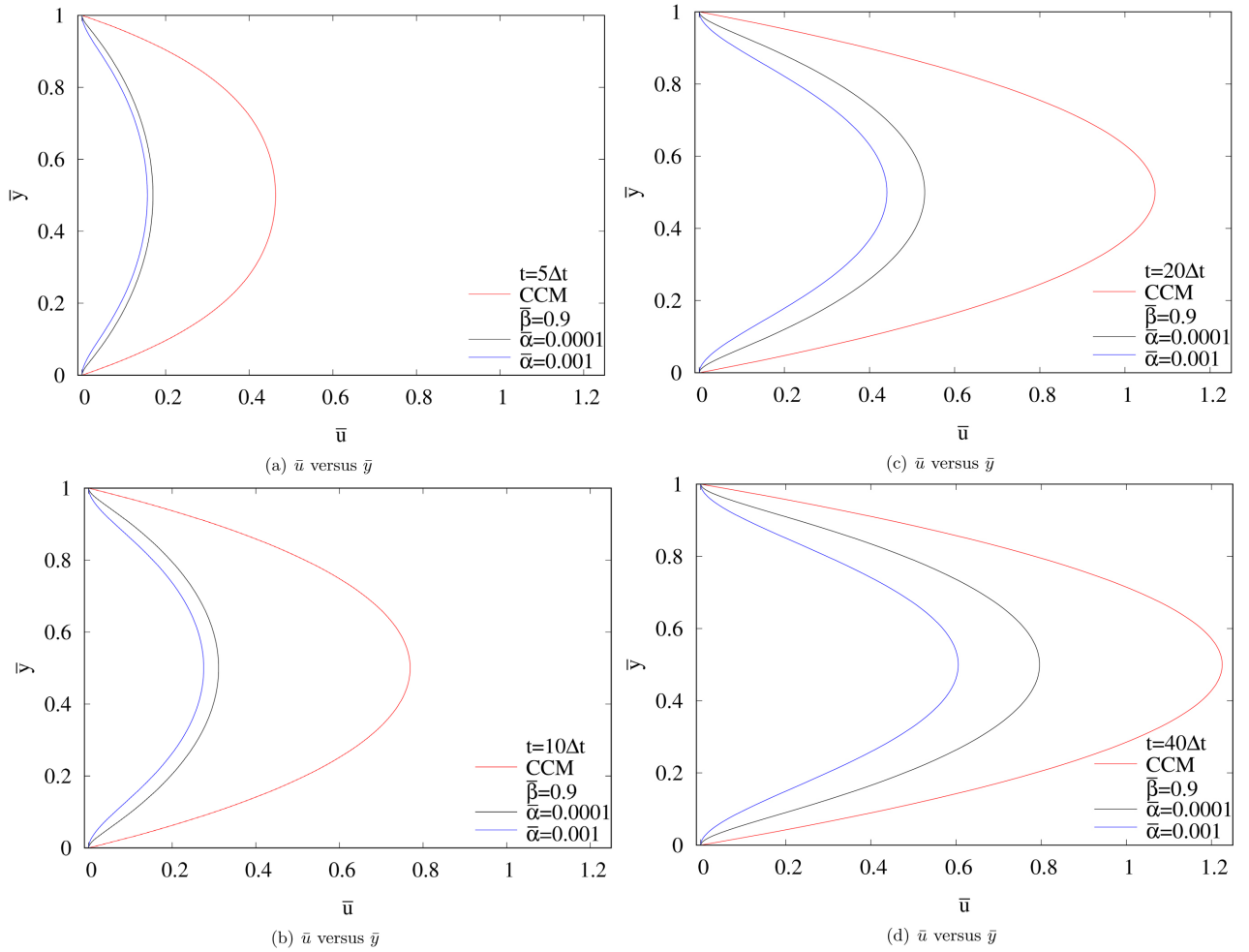

(a) $\bar{u}$ versus $\bar{y}$ (c) $\bar{u}$ versus $\bar{y}$

(b) $\bar{u}$ versus $\bar{y}$ (d) $\bar{u}$ versus $\bar{y}$

Figure 12. Developing flow between parallel plates: velocity $\bar{u}$ versus position $\bar{y}$: Models A and C (Case II), $\bar{\beta}=0.9$.

evolution, demonstrating increasing resistance to flow with increasing value of $\bar{\alpha}$ during the entire evolution.

Case B

In case B we present two studies. In the first study, we choose

Model A (CCM): $Re=5$

Model C (NCCM): $Re=5$; $\bar{\alpha}=0.01,0.1$; $\bar{\beta}=0.05,0.2$

Computations are performed using the same mesh and other details as in case A. **Figures 16(a)-(d)** show plots of evolution of $\bar{u}$ versus $\bar{y}$ at $t=5\Delta t$ and $t=20\Delta t$ for $\bar{\beta}=0.05$ and $\bar{\beta}=0.2$ for both values of $\bar{\alpha}$ in each case. Once again, combination of higher values of $\bar{\alpha}$ and $\bar{\beta}$ result in more reduction in the velocity due to higher resistance to flow. Velocities for $\bar{\beta}=0.2$ are lower than those for $\bar{\beta}=0.05$ for both values of $\bar{\alpha}$. In the second study, we choose a fixed $\bar{\alpha}=0.1$ and vary $\bar{\beta}=0.1,0.2,0.3$. **Figure 17(a)** and **Figure 17(b)** shows evolution of $\bar{u}$ versus $\bar{y}$ at $t=\Delta t$ and $t=5\Delta t$. Progressively increasing values of $\bar{\beta}$ results in progressively reduced values of velocity $\bar{u}$. **Figures 18(a)-(c)** show evolution of ${}_i\bar{\omega}_3$ versus $\bar{y}$ for: Model A, CCM ($Re=5$); Model B, NCCM ($Re=5$, $\bar{\alpha}=0.001$) and Model C, NCCM ($Re=5$, $\bar{\alpha}=0.001$ and

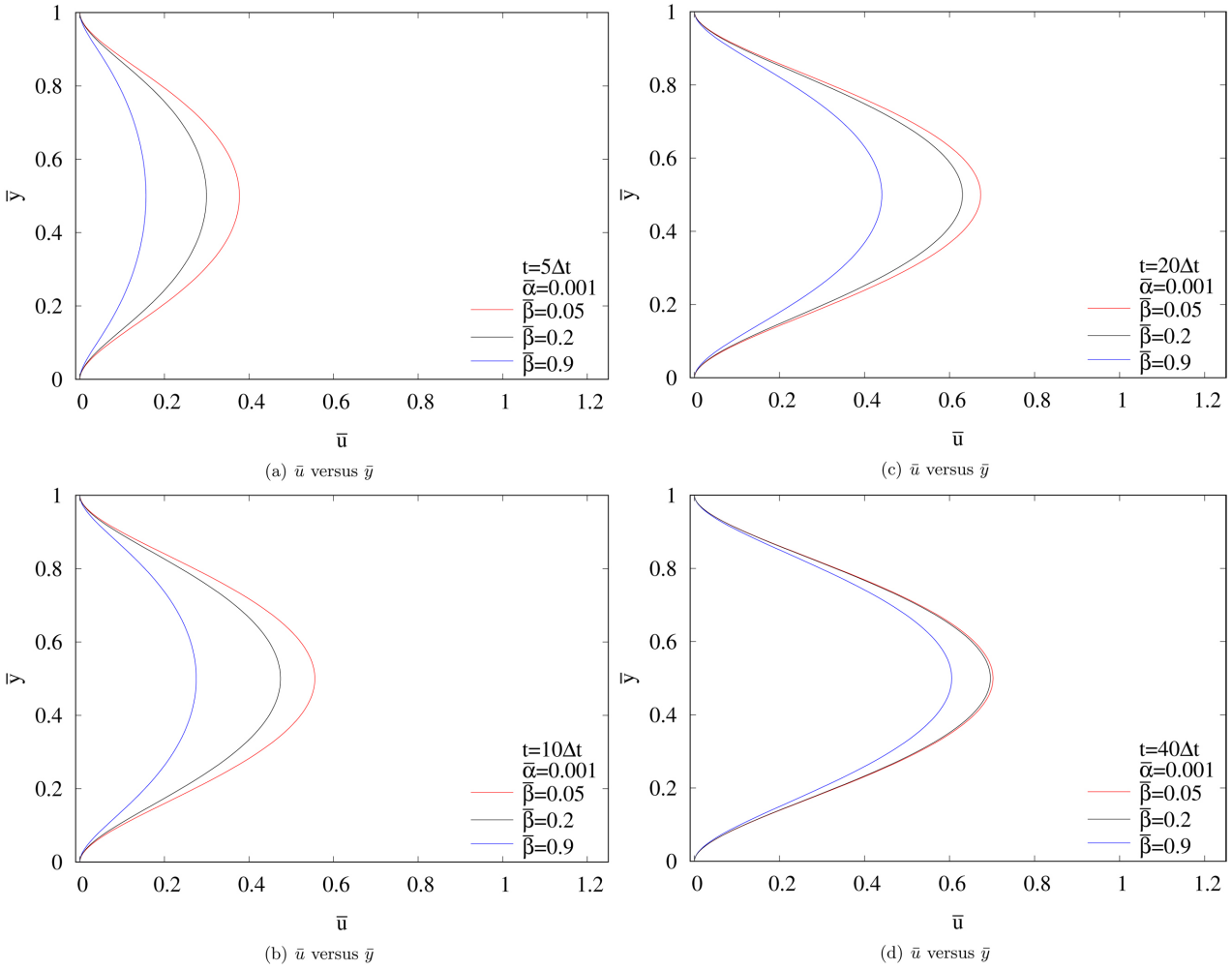

Figure 13. Developing flow between parallel plates: velocity $\bar{u}$ versus position $\bar{y}$: Model C (Case III).

$\bar{\beta}=0.05$). Corresponding ${}_s\bar{m}_{23}$ versus $\bar{y}$ graphs are shown in **Figures 19(a)-(c)**. In **Figure 18(a)** and **Figure 18(b)** we clearly observe the change in ${}_i\bar{\omega}_3$ free field due to micropolar physics. In **Figure 18(c)**, we observe further reduction and change in ${}_i\bar{\omega}_3$ due to $\bar{\beta}=0.05$. Evolution of ${}_s\bar{m}_{23}$ versus $\bar{y}$ follows a trend opposite to ${}_i\bar{\omega}_3$ *i.e.*, $\bar{\alpha}\neq 0$ introduces nonzero ${}_s\bar{m}_{23}$ and introduction of $\bar{\beta}$ further changes evolution of existing nonzero ${}_s\bar{m}_{23}$ due to only $\bar{\alpha}$.

3.2.2. Remarks

1) In this work, $\bar{\alpha}$ and $\bar{\beta}$ are two parameters related to the micropolar physics. We have seen in the model problem studies that both offer increasing resistance to flow with their increasing values.

2) Model problem studies show that resistance to flow due to $\bar{\beta}$ (${}^{\Theta}\bar{I}$ and $\bar{\rho}$ combined) is more pronounced compared to $\bar{\alpha}$.

3) Parameters $\bar{\alpha}$ and ${}^{\Theta}\bar{I}$ are properties of the micropolar medium controlled by the microconstituents, but the manner in which they exert their influence on flow physics is different. The parameter $\bar{\alpha}$ is a measure of the

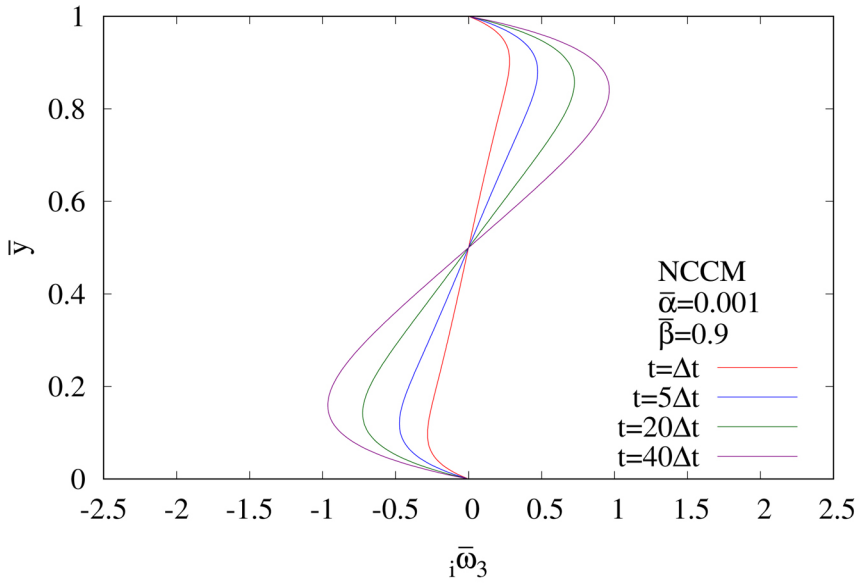

(a) $\bar{u}$ versus $\bar{y}$

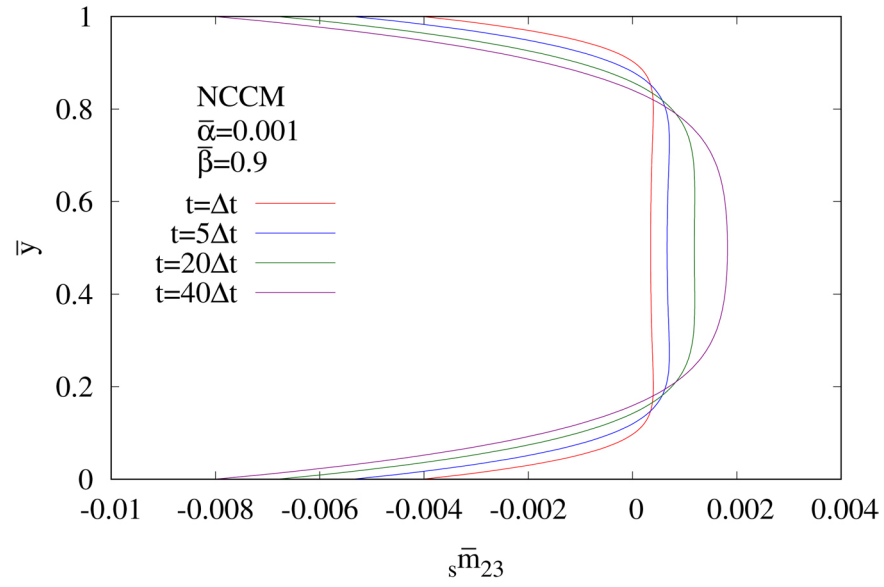

(b) $\bar{u}$ versus $\bar{y}$

Figure 14. Developing flow between parallel plates: Model B (Case II): $_i\bar{\omega}_3$ and $_s\bar{m}_{23}$ versus $\bar{y}$: $\bar{\alpha}=0.001$, $\bar{\beta}=0.9$.

collective resistance offered to the flow by each microconstituents. Whereas $^{\Theta}\bar{I}$ appears as $^{\Theta}\bar{I}\bar{\rho}$, suggesting that it is a volumetric or mass effect through angular acceleration. Thus $^{\Theta}\bar{I}\bar{\rho}$ is the collective influence of a group of microconstituents in a unit volume and perhaps provides a better explanation of why $\bar{\beta}$ is more influential than $\bar{\alpha}$.

4. Summary and Conclusions

The micropolar NCCT for solids derived using internal rotations (due to deformation gradient tensor) with rotational inertial physics [3] and the micropolar

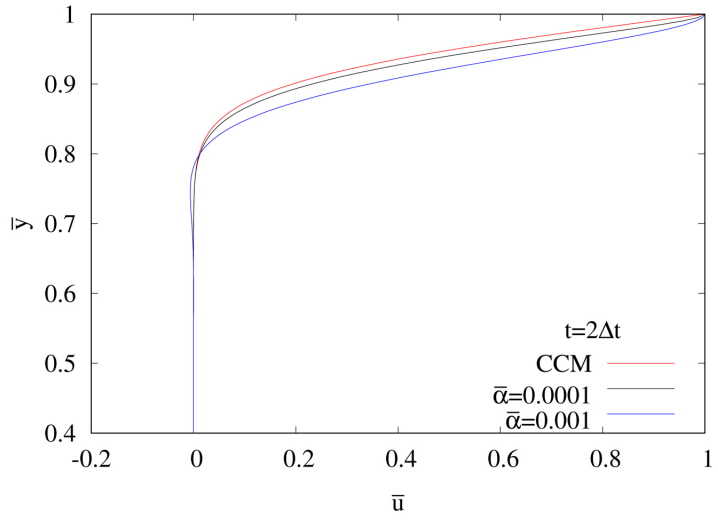

(a) $\bar{u}$ versus $\bar{y}$

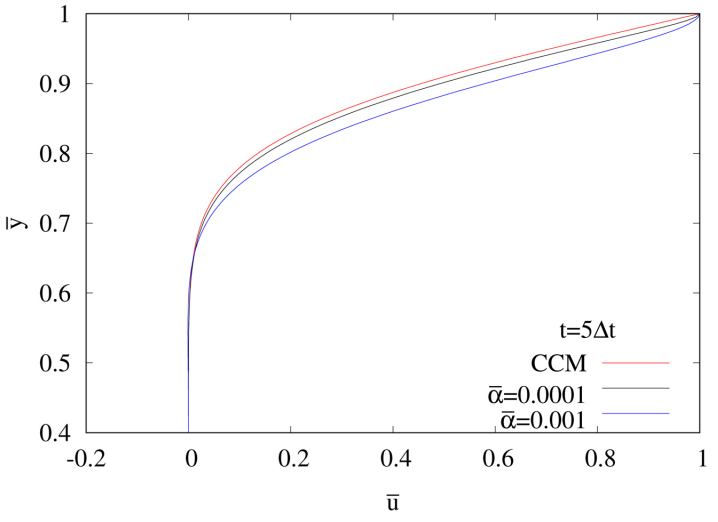

(b) $\bar{u}$ versus $\bar{y}$

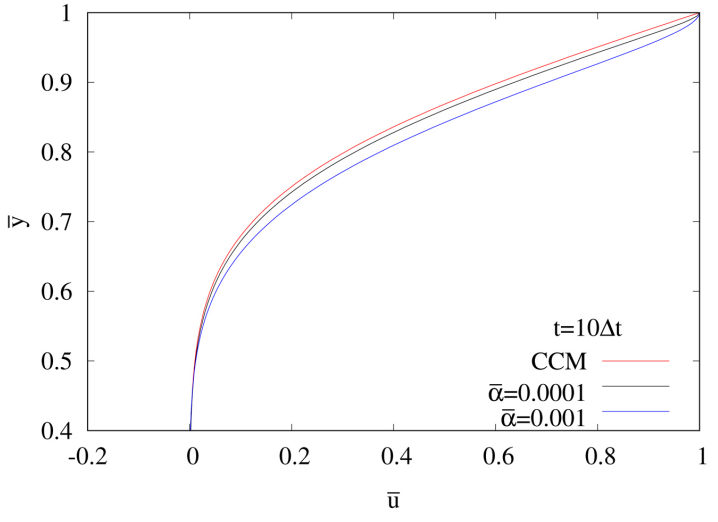

(c) $\bar{u}$ versus $\bar{y}$

Figure 15. Developing Couette flow: velocity $\bar{u}$ versus position $\bar{y}$: Models A and B (Case A).

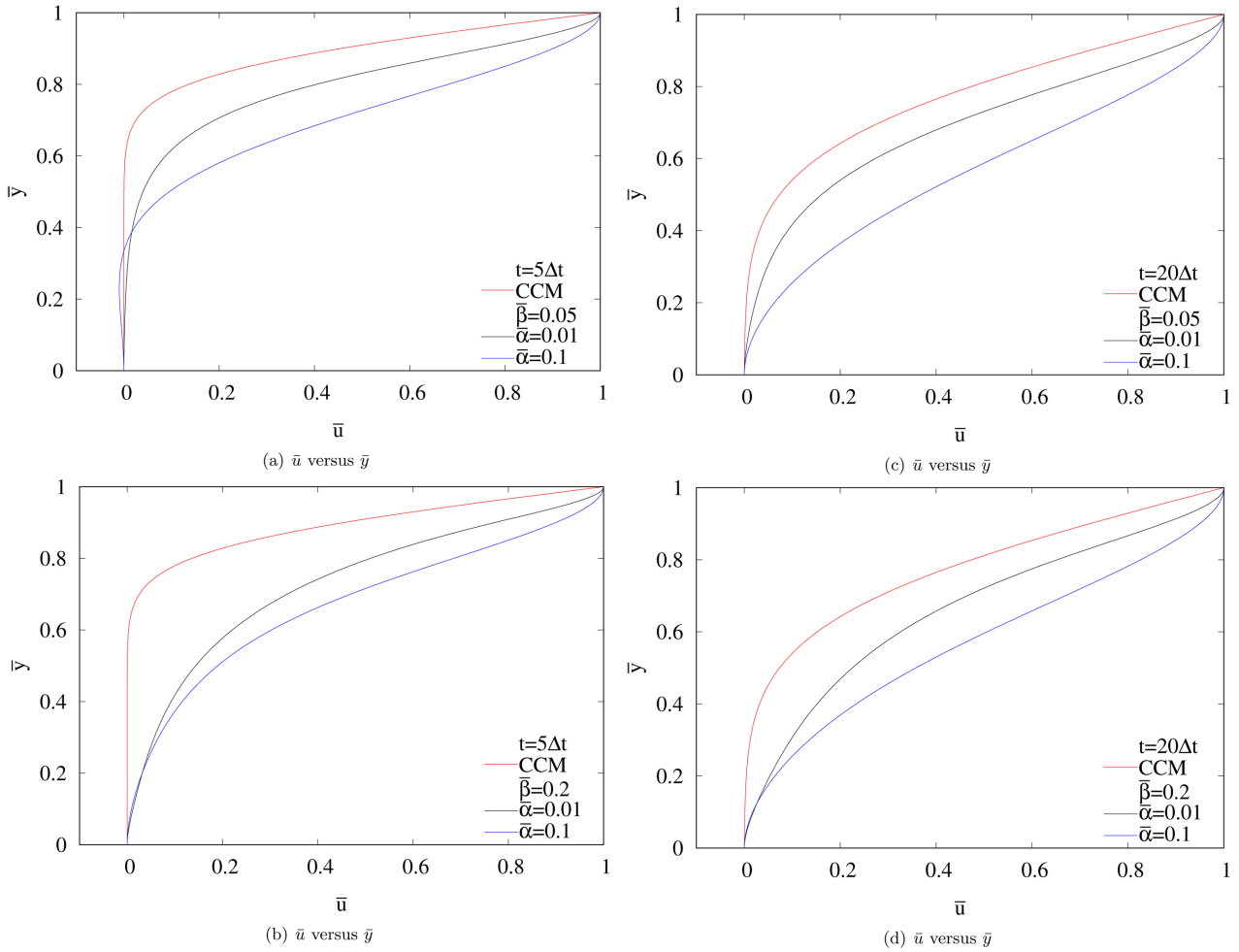

(a) $\bar{u}$ versus $\bar{y}$ (c) $\bar{u}$ versus $\bar{y}$

(b) $\bar{u}$ versus $\bar{y}$ (d) $\bar{u}$ versus $\bar{y}$

Figure 16. Developing Couette flow: velocity $\bar{u}$ versus position $\bar{y}$: Models A and C (Case B).

NCCT for fluids derived using internal rotation rates (due to velocity gradient tensor) with rotational inertial physics [4] are considered in the work presented in this paper, to present various model problem studies that illustrate the influence of rotational inertial physics in case of micropolar solids as well as micropolar fluids. In this section, we present a summary of the work and draw some conclusions from it.

1) In reference [3], by examining the BLM and BAM for micropolar solids with NCCT based on internal rotations, authors established co-existence of translational and rotational waves in micropolar solids with small deformation, small strain physics.

2) In reference [4], authors considered BLM and BAM of the micropolar NCCT for fluids to show that in this case neither translational nor rotational waves can exist due to absence of elasticity or stiffness due to absence of strain physics in both CCM as well as NCCM.

3) Conclusions (1) and (2) in references [3] [4] were purely based on mathematical model. Solutions of IVPs resulting from the conservation and balance laws and the constitutive theories were not presented.

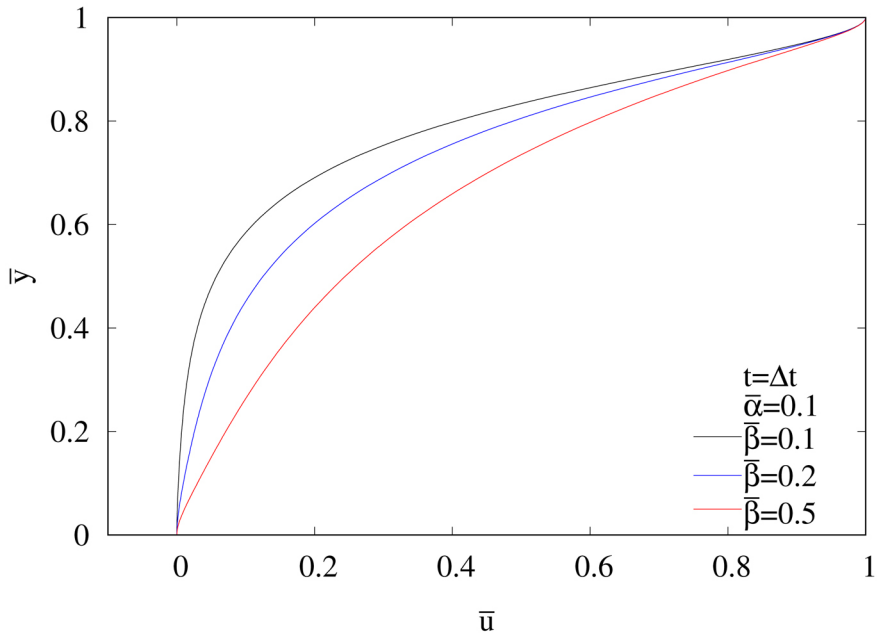

(a) $\bar{u}$ versus $\bar{y}$

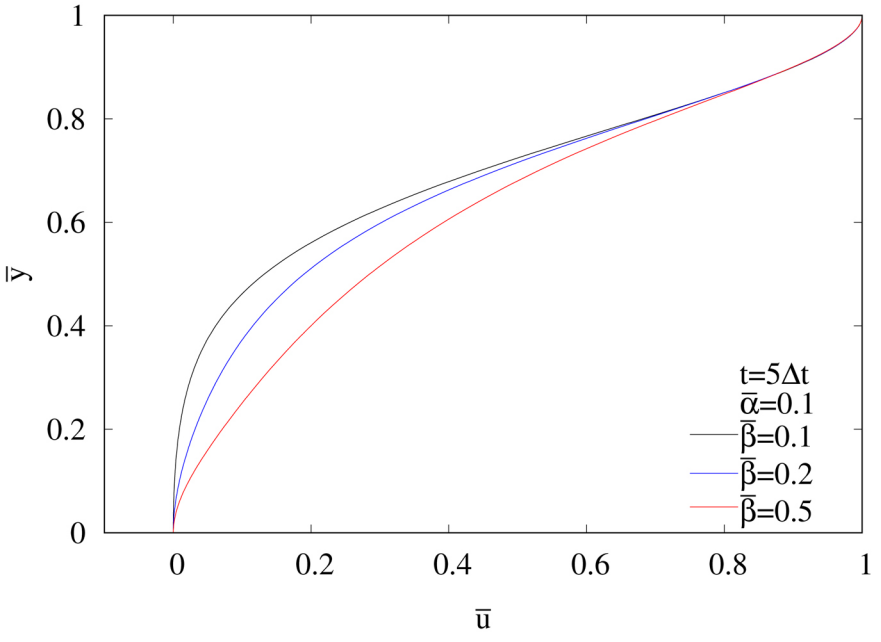

(b) $\bar{u}$ versus $\bar{y}$

Figure 17. Developing Couette flow: velocity $\bar{u}$ versus position $\bar{y}$: (Case B, second study).

4) In this paper, we consider the mathematical models of reference [3] [4] with rotational inertial physics to construct model problems (IVPs) and present their solutions using space-time coupled finite element method. The model problems are intentionally kept simple so that significant aspects of the micro-polar physics due to microconstituents and in particular influence of rotational inertial physics can be demonstrated clearly.

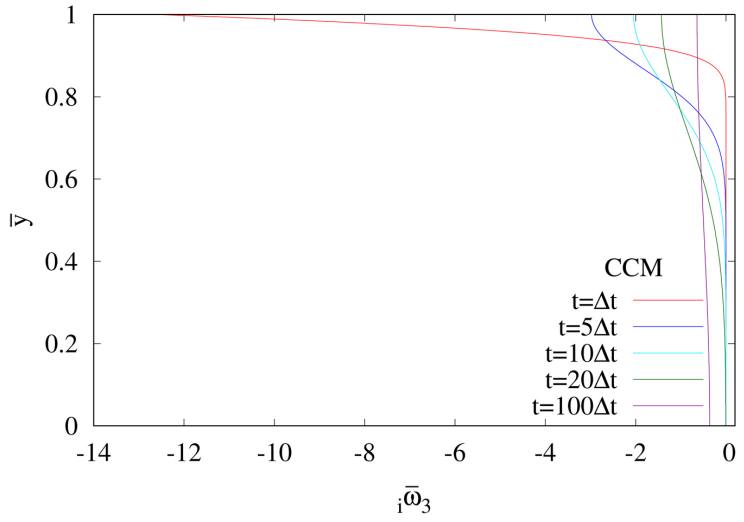

(a) $_i\bar{\omega}_3$ versus $\bar{y}$

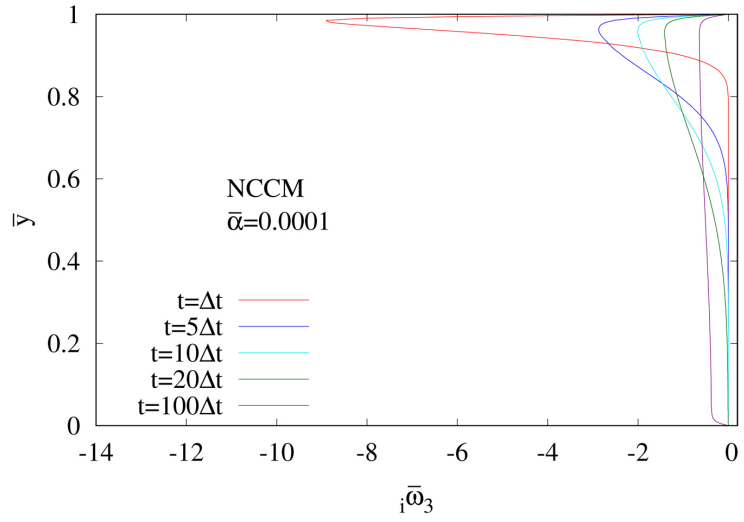

(b) $_i\bar{\omega}_3$ versus $\bar{y}$

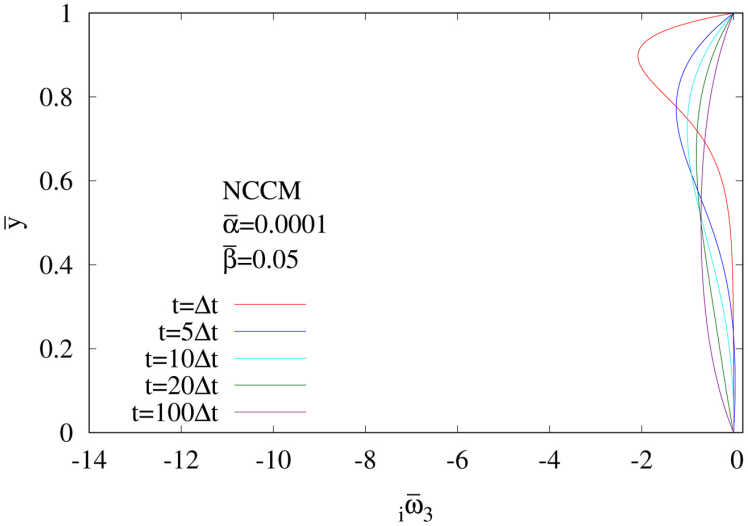

(c) $_i\bar{\omega}_3$ versus $\bar{y}$

Figure 18. Developing Couette flow: $_i\bar{\omega}_3$ versus $\bar{y}$: Models A, B and C.

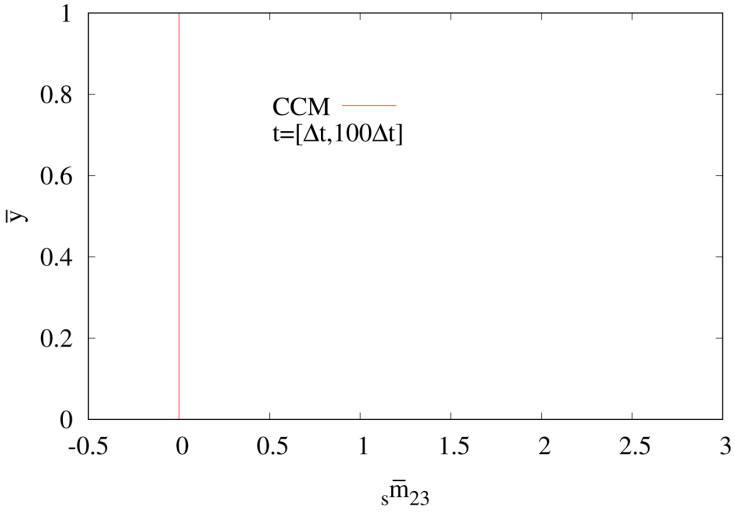

(a) $_s\bar{m}_{23}$ versus $\bar{y}$

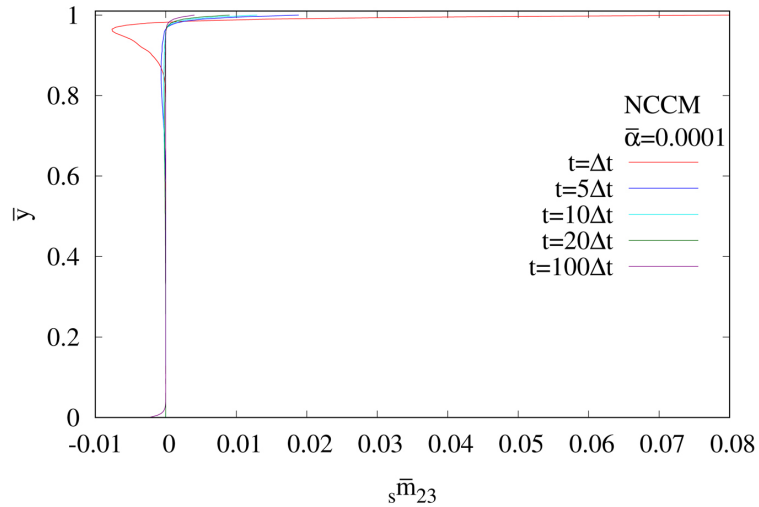

(b) $_s\bar{m}_{23}$ versus $\bar{y}$

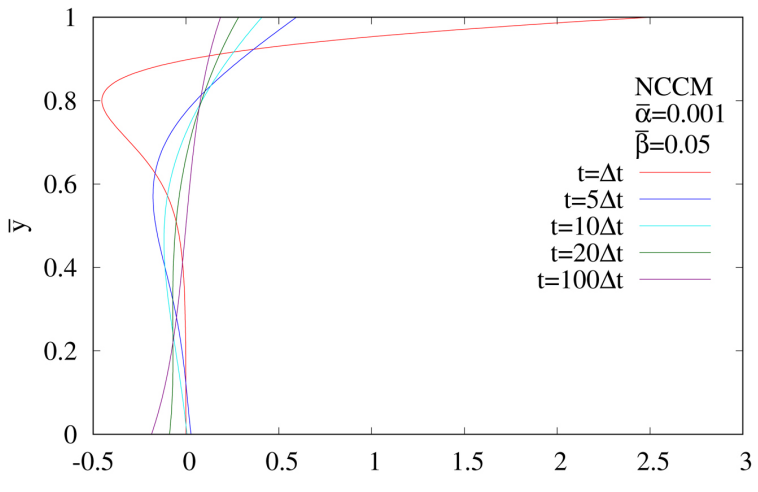

(c) $_s\bar{m}_{23}$ versus $\bar{y}$

Figure 19. Developing Couette flow: $_i\bar{\omega}_3$ versus $\bar{y}$: Models A, B and C. Developing Couette flow: $_s\bar{m}_{23}$ versus $\bar{y}$: Models A, B and C.

5) The solutions of the model problems (IVPs) are obtained by using space-time coupled finite element method based on space-time residual functional for a space-time strip with time marching. The space-time local approximation are p-version hierarchical in space and time with higher order global differentiability in space and time. In this approach, with the choice of minimally confirming spaces, when the space-time residual functional for a space-time strip is $O(10^{-8})$ or lower, PDEs in the IVPs are satisfied accurately, hence the computed evolutions are almost time accurate.

6) In the present work, we consider micropolar NCCT of references [3] [4] but with dissipation mechanisms due to: strain rate (CCM) and due to rate of symmetric part of internal rotational gradient tensor (Micropolar nonclassical dissipation). While the strain rate dissipation (CCT) is viscous, the nonviscous dissipation mechanisms in micropolar NCCT is due to microconstituents and the fluid medium. These aspects were not considered in the micropolar NCCT in references [3] [4], hence is additional new physics in the mathematical models.

7) From the one dimensional numerical studies presented for translational and rotational waves in micropolar solid medium using Models TW1, RW1 and RW2 we observe:

a) Existence and propagation of translational wave (CCM) in the absence and in the presence of strain rate dissipation. The translational wave propagates, reflects, the reflected wave propagates and reflects from the free boundary without amplitude decay and base elongation when the medium is inviscid. The same phenomenon exists in the presence of damping but with continued amplitude decay and base elongation during evolution. Amplitude decay is most pronounced for the incident wave where as base elongation is more prominent in the reflected waves.

b) In the case of Model RW1, in which the rotational wave speed is one, the evolution of rotational wave physics is exactly same as in Model TW1.

c) Model RW2 permits the choice of wave speed. Studies for wave speed faster than one and slower than one with and without dissipation are presented. In 2D and 3D applications choice of t_0 using v_0/L_0 or ${}_i\omega_0/L_0$ permits translational wave speed of one or rotational wave speed of one, but both wave speeds cannot be one. In this study, we show that wave speed different than one only influences when the propagating wave reaches the boundaries. The studies conclusively demonstrate that rotational inertial physics in micropolar solids is essential for the existence of rotational waves in micropolar solids.

d) In the studies presented here, rotational and translational waves are decoupled but coexist. In $\mathbf{R}^2$ and $\mathbf{R}^3$ this is not the case (Section 3.1.1). Since translational waves depend upon gradients of displacements in $\left[{}^{d}_{s}J\right]$ and the rotational waves depend upon the gradients of displacements in $\left[{}^{d}_{a}J\right]$, both $\left[{}^{d}_{s}J\right]$ and $\left[{}^{d}_{a}J\right]$ being due to $\left[J\right]$, we expect coupling in the two in $\mathbf{R}^2$ and $\mathbf{R}^3$.

e) Both micropolar and non-micropolar media are assumed isotropic and homogeneous, thus this micropolar theory can not simulate wave dispersion in micropolar media due to microconstituents. This theory can only simulate the influence of micropolar physics on wave propagation physics without dispersion.

8) In the case of micropolar fluid, neither translational nor rotational waves exist. The 1D form of BAM in this case is a time dependent diffusion equation. Two numerical studies are presented for two values of diffusion coefficient. From the studies, we clearly see higher values of the diffusion coefficient result in faster diffusion of the applied pulse.

9) Numerical studies presented for pressure driven developing flow between parallel plates show:

a) Micropolar physics with increasing $\bar{\alpha}$ ($\bar{\beta}=0$) results in progressively increasing resistance to flow and progressively decreasing flow rate. This holds during the entire evolution for each value of time.

b) We have shown that $\bar{\beta}$, which controls rotational inertial physics, also offers resistance to flow. Increasing values of $\bar{\beta}$ results in decreasing flow rate.

c) Thus, in micropolar fluids with both $\bar{\alpha}$ and $\bar{\beta}$, the resulting flow rate is decreased. Since the constitutive model is not calibrated their relative influence on the flow rate is difficult to ascertain. Based on the values of $\bar{\alpha}$ and $\bar{\beta}$ used, $\bar{\beta}$ influences flow rate more than $\bar{\alpha}$. We have discussed the physics related to $\bar{\alpha}$ and $\bar{\beta}$ in Section 3.2.2. Both $\bar{\alpha}$ and $\bar{\beta}$ offer resistance to flow but the physics of the resistance mechanisms is different in the two cases.

d) The significance of these studies is that we can conclusively see that rotational inertial physics in micropolar nonclassical continuum theories for fluids offers further resistance to the motion of the fluids over and beyond rotation rates or rotation rate gradients, thus reducing velocities and flow rates.

10) Numerical studies presented for Couette flow confirms the findings reported in item (9).

11) Presence of rotational inertial physics in fluids only offers added resistance to fluid motion. It can not possibly result in rotational waves as micropolar fluids have no elasticity associated with micropolar physics. In the case of micropolar fluids, BAM is not a wave equation in rotation rate.

12) Evolution of ${}_i\bar{\omega}_3$ versus $\bar{y}$ and ${}_s\bar{m}_{23}$ versus $\bar{y}$ (**Figure 10(a)** and **Figure 10(b)**) for Model A (CCM) and their comparison with similar evolution when $\bar{\alpha}=0.001$ ($\bar{\beta}=0.0$) *i.e.*, model B shown in **Figure 10(c)** and **Figure 10(d)** and those for $\bar{\alpha}=0.001$ and $\bar{\beta}=0.9$ in **Figure 14(a)** and **Figure 14(b)** clearly demonstrate how the free field ${}_i\bar{\omega}_3$ and zero ${}_s\bar{m}_{23}$ in **Figure 10(a)** and **Figure 10(b)** are affected by the presence of microconstituents without and with rotational inertial physics. These studies show that increasing $\bar{\alpha}$ ($\bar{\beta}=0.0$) reduces ${}_i\bar{\omega}_3$ field due to resistance offered by the microconstituents. When both $\bar{\alpha}$ and $\bar{\beta}$ are nonzero, resistance offered by the microconstituents increases resulting in further reduction in ${}_i\bar{\omega}_3$ field. The consequences of reducing ${}_i\bar{\omega}_3$

field are increase in ${}_s\bar{m}_{23}$ as shown in the graphs.

Acknowledgements

First author is grateful for his endowed professorship and the department of mechanical engineering of the University of Kansas for providing financial support to the second author. The computational facilities provided by the Computational Mechanics Laboratory of the mechanical engineering department are also acknowledged.

Conflicts of Interest

The authors declare no conflicts of interest regarding the publication of this paper.

References

[1] Surana, K.S. and Mathi, S.S.C. (2023) Thermodynamic Consistency of Nonclassical Continuum Theories for Solid Continua Incorporating Rotations. *Continuum Mechanics and Thermodynamics*, **35**, 17-59. https://doi.org/10.1007/s00161-022-01163-y

[2] Surana, K.S. and Carranza, C.H. (2022) Nonclassical Continuum Theories for Fluent Media Incorporating Rotation Rates and Their Thermodynamic Consistency. *ZAMM—Journal of Applied Mathematics and Mechanics*, **103**, e202200079. https://doi.org/10.1002/zamm.202200079

[3] Surana, K.S. and Kendall, J.K. (2020) Existence of Rotational Waves in Non-Classical Thermoelastic Solid Continua Incorporating Internal Rotations. *Continuum Mechanics and Thermodynamics*, **32**, 1659-1683. https://doi.org/10.1007/s00161-020-00872-6

[4] Surana, K.S. and Kendall, J.K. (2022) Rotational Inertial Physics in Non-Classical Thermoviscous Fluent Continua Incorporating Internal Rotation Rates. *Applied Mathematics*, **13**, 453-487. https://doi.org/10.4236/am.2022.136030

[5] Islam, M., Nasrin, S. and Alam, M. (2020) Unsteady Electromagnetic Free Convection Micropolar Fluid Flow through a Porous Medium along a Vertical Porous Plate. *Open Journal of Applied Sciences*, **10**, 701-718. https://doi.org/10.4236/ojapps.2020.1011049

[6] Koriko, O., Omowaye, A., Popoola, A., Oreyeni, T., Adegbite, A., Oni, E., Omokhuale, E. and Altine, M. (2022) Insight into Dynamics of Hydromagnetic Flow of Micropolar Fluid Containing Nanoparticles and Gyrotactic Microorganisms at Weak and Strong Concentrations of Microelements: Homotopy Analysis Method. *American Journal of Computational Mathematics*, **12**, 267-282. https://doi.org/10.4236/ajcm.2022.122017

[7] Surana, K.S. and Reddy, J.N. (2017) The Finite Element Method for Initial Value Problems. CRC/Taylor and Francis, Boca Raton, FL. https://doi.org/10.1201/b22512

[8] Surana, K.S., Powell, M.J. and Reddy, J.N. (2015) A More Complete Thermodynamic Framework for Fluent Continua. *Journal of Thermal Engineering*, **1**, 460-475. https://doi.org/10.18186/jte.00314

[9] Surana, K.S., Powell, M.J. and Reddy, J.N. (2015) A Polar Continuum Theory for Fluent Continua. *International Journal of Engineering Research and Industrial Applications*, **8**, 107-146.

Nomenclatures

α_1^* Diffusion coefficient in Model RW2

α_1, α_2 Material coefficient for constitutive theory for Cauchy moment tensor

$\bar{\alpha}$ Nonclassical physics material coefficient

α_0 Dimensionless nonclassical physics material coefficient

$\bar{\beta}$ Rotational inertial physics nonclassical material coefficient

$\bar{c}_2$ Dimensionless dissipation coefficient fluids

c_d Damping coefficient Model TW1

c_d^* Damping coefficient Model RW1, RW2

E Modulus of elasticity

E_0 Reference modulus of elasticity

e Specific internal energy in Lagrangian description

$\bar{e}$ Specific internal energy in Eulerian description

ϵ, $\boldsymbol{\epsilon}$, ϵ_{ijk} Permutation tensor

$\boldsymbol{\varepsilon}$ Strain tensor in Lagrangian description

$\bar{\boldsymbol{\varepsilon}}$ Strain tensor in Eulerian description

$\dot{\boldsymbol{\varepsilon}}$ Strain rate tensor in Lagrangian description

$\dot{\bar{\boldsymbol{\varepsilon}}}$ Strain rate tensor in Eulerian description

η Viscosity in Lagrangian description

$\bar{\eta}$ Viscosity in Eulerian description

$\boldsymbol{g}$ Heat vector in Lagrangian description

$\bar{\boldsymbol{g}}$ Heat vector in Eulerian description

${}^{\Theta}I$ Internal rotational inertia in Lagrangian description

${}^{\Theta}\bar{I}$ Internal rotational inertia in Eulerian description

$\boldsymbol{J}$ Deformation gradient tensor in Lagrangian description

${}_s\boldsymbol{J}$ Symmetric part of deformation gradient tensor in Lagrangian description

${}_a\boldsymbol{J}$ Skew Symmetric part of deformation gradient tensor in Lagrangian description

${}^d\boldsymbol{J}$ Displacement gradient tensor in Lagrangian description

${}^d_s\boldsymbol{J}$ Symmetric part of displacement gradient tensor in Lagrangian description

${}^d_a\boldsymbol{J}$ Skew symmetric part of displacement gradient tensor in Lagrangian description

L, L_0 Length, reference length

$\boldsymbol{L}$, $\dot{\boldsymbol{J}}$ Velocity gradient tensor in Lagrangian description

$\bar{\boldsymbol{L}}$ Velocity gradient tensor in Eulerian description

${}_s m_{11}$ Symmetric Cauchy moment tensor in Lagrangian description component 11

${}_s \bar{m}_{11}$ Symmetric Cauchy moment tensor in Eulerian description component 11

${}_s \bar{m}_{23}$ Symmetric Cauchy moment tensor in Eulerian description component 23

${}_a \bar{m}_{23}$ Skew symmetric Cauchy moment tensor in Eulerian description component 23

${}_i\boldsymbol{\omega}$, ${}_i\omega_k$ Internal rotational velocity or rotation rates

${}_i\omega_1$ Internal rotation rate in Lagrangian description about the x_1 axis

ω_0 Reference rotational velocity

${}_i\bar{\omega}_1$ Internal rotation rate in Eulerian description about the x_1 axis

${}_i\bar{\omega}_3$ Internal rotation rate in Eulerian description about the x_3 axis

$\bar{\Omega}_{xt}$ Space-time domain

$\bar{\Omega}_{xt}^{T}$ Discretization of space-time domain $\bar{\Omega}_{xt}$

$\bar{\Omega}_{xt}^{(i)}$ i^{th} space-time strip

$\left(\bar{\Omega}_{xt}^{(i)}\right)^{T}$ Discretization of i^{th} space-time strip

$\bar{\Omega}_{xt}^{e}$ Space-time element e

ρ_0 Reference Density

ρ Density in Lagrangian description

$\bar{\rho}$ Density in Eulerian description

$\bar{p}$ Pressure in Eulerian description

$\boldsymbol{\sigma}$ Cauchy stress tensor in Lagrangian description

${}_{s}\boldsymbol{\sigma}$ Symmetric Cauchy stress tensor in Lagrangian description

${}_{a}\boldsymbol{\sigma}$ Skew symmetric Cauchy stress tensor in Lagrangian description

${}_{s}^{e}\boldsymbol{\sigma}$ Symmetric equilibrium Cauchy stress tensor in Lagrangian description

${}_{s}^{d}\boldsymbol{\sigma}$ Symmetric deviatoric Cauchy stress tensor in Lagrangian description

${}_{s}^{d}\bar{\sigma}_{21}^{(0)} = {}_{s}^{d}\bar{\sigma}_{12}^{(0)}$ Symmetric deviatoric contravariant Cauchy stress in Eulerian description component 12

${}_{a}^{d}\bar{\sigma}_{21}^{(0)} = {}_{a}^{d}\bar{\sigma}_{12}^{(0)}$ Antisymmetric deviatoric contravariant Cauchy stress in Eulerian description component 12

t Time

t_0 Reference time

τ_0 Reference stress

${}_{i}\boldsymbol{\Theta}$, ${}_{i}\Theta_{j}$, $\left\{{}_{i}\Theta\right\}$ Internal or classical rotations in Lagrangian description

${}_{i}\bar{\boldsymbol{\Theta}}$, ${}_{i}\bar{\Theta}_{j}$, $\left\{{}_{i}\bar{\Theta}\right\}$ Internal or classical rotations in Eulerian description

${}_{i}^{r}\boldsymbol{\Theta}$ Internal or classical rotation rates in Lagrangian description

${}_{i}^{r}\bar{\boldsymbol{\Theta}}$ Internal or classical rotation rates in Eulerian description

${}_{i}\Theta_1$ Internal rotation about the x_1 axis

${}_{i}\Theta_3$ Internal rotation about the x_3 axis

$\bar{u}$, $\bar{v}$, $\bar{w}$ Velocity components in x_1, x_2 and x_3 directions

v_0 Reference velocity

$\boldsymbol{v}$, v_i, $\{v\}$ Velocity vector in Lagrangian description

$\bar{\boldsymbol{v}}$, $\bar{v}_i$, $\{\bar{v}\}$ Velocity vector in Eulerian descriptions

$\boldsymbol{x}$, x_i, $\{x\}$ Cartesian Coordinates

$\bar{\boldsymbol{x}}$, $\bar{x}_i$, $\{\bar{x}\}$ Cartesian Coordinates

y Cartesian Coordinates

$\bar{y}$ Cartesian Coordinates

Abbreviations

BAM: Balance of angular momentum
BLM: Balance of linear momentum
BMM: Balance of moment of moments
BVP: Boundary value problem
CBL: Conservation and balance laws
CCM: Classical continuum mechanics
CCT: Classical continuum theory
CM: Conservation of mass
FLT: First law of thermodynamics
IVP: Initial value problem
NCCM: Non-classical continuum mechanics
NCCT: Non-classical continuum theory
ODE: Ordinary differential equation
PDE: Partial differential equation
SLT: Second law of thermodynamics